STATE RESEARCH CENTER OF RUSSIA

INSTITUTE FOR HIGH ENERGY PHYSICS

IHEP 99-14

C.Allgower[1], M.Bai[4,c], V.Baturine[8,e], N.I.Belikov[3], G.Bunce[2], A.A.Derevschikov[3], H.En'yo[6], V.Ghazikanian[9], Y.Goto[5], N.Hayashyi[5], H.Huang[2], T.Ichihara[5], G.Igo[9], K.Imai[6], T.Kasprzyk[1], Y.Kondo[6], K.Krueger[1], S.Y.Lee[4], Y.Makdisi[2], Yu.A.Matulenko[3], Y.Nakada[6,d], L.V.Nogach[3,b], S.B.Nurushev[3], A.Ogawa[8], H.Okamura[7], M.Okamura[5], A.I.Pavlinov[3], T.Roser[2], N.Saito[5], H.Sakai[7], H.Sato[6], H.Spinka[1], M.Syphers[2,a], S.Trentalange[9], D.Underwood[1], A.N.Vasiliev[3], T.Wakasa[7], C.Whitten[9], A.Yokosawa[1]

MEASUREMENT OF SINGLE-SPIN ASYMMETRIES OF π^+, π^-, AND PROTONS INCLUSIVELY PRODUCED ON A CARBON TARGET WITH A 21.6 GEV/C INCIDENT POLARIZED PROTON BEAM (BNL E925 Experiment)

[1]Argonne National Laboratory, Argonne, Illinois 60439, USA

[2]Brookhaven National Laboratory, Upton, New York 11973, USA

[3]Institute for High Energy Physics, Protvino 142284, Russia

[4]Indiana University, Bloomington, Indiana 47405, USA

[5]RIKEN, The Institute of Physical and Chemical Research, Japan

[6]Department of Physics, Kyoto University, Japan

[7]Department of Physics, University of Tokio, Japan

[8]Pennsylvania State University, University Park, Pennsylvania 16802, USA

[9]UCLA, Los Angeles, California 90095, USA

[a]Present address: Fermi National Accelerator Laboratory, Batavia, Illinois 60510, USA

[b]Also associated with Moscow State University, Moscow, Russia

[c]Partially supported by Argonne National Laboratory, Argonne, Illinois 60439, USA

[d]Present address: Toshiba Corporation, Tokyo, Japan

[e]Also associated with PNPI, St.Petersburg, Russia

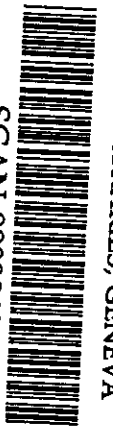

Protvino 1999

UDK 539.171

M–24

Abstract

Allgower C. et al. Measurement of single-spin asymmetries of π^+, π^-, and protons inclusively produced on a carbon target with a 21.6 GeV/c incident polarized proton beam. (BNL E925 Experiment): IHEP Preprint 99-14. – Protvino, 1999. – p. 32, figs. 17, tables 14, refs.: 29.

The single-spin asymmetry, A_N, in inclusive $\pi^{\pm}$-production has been measured using a 21.6 GeV/c transversely-polarized proton beam on a carbon target. A large A_N was found for $x_F > 0.5$ and for $0.6 < p_T < 1.2$ GeV/c, with similar magnitudes and opposite signs for π^+ and π^-. The A_N for inclusive proton production has also been measured and is consistent with zero.

Аннотация

Аллговер К. и др. Измерение односпиновой асимметрии в инклюзивном образовании π^+, π^- и протонов на углеродной мишени с использованием поляризованного протонного пучка с импульсом 21.6 GeV/c. (Эксперимент E925 БНЛ): Препринт ИФВЭ 99-14. – Протвино, 1999. – 32 с., 17 рис., 14 табл., библиогр.: 29.

Измерена односпиновая асимметрия A_N в инклюзивном образовании $\pi^{\pm}$ на углеродной мишени с использованием поперечно поляризованного протонного пучка с импульсом 21.6 GeV/c. Для π^+ и π^- обнаружены значительные асимметрии в области $x_F > 0.5$ и $0.6 < p_T < 1.2$ГэВ/c, близкие по величине и противоположные по знаку. Также была измерена A_N в инклюзивном образовании протонов, ее величина сравнима с нулем во всей кинематической области.

1. INTRODUCTION

RHIC, the heavy ion collider being built at Brookhaven, offers an exciting opportunity to collide highly polarized protons at such high energy and luminosity as 500 GeV and 2×10^{32} cm^2/sec. The accesible physics includes study of the spin content of a proton, particularly gluon and antiquark polarization, study of large PQCD-predicted asymmetries for parton-parton subprocesses, and parity violation search and study. A beam polarization at RHIC is expected to be about 70% and has to be measured in the range from 23 GeV injection energy up to 250 GeV. The RHIC polarimeter, that is setup to measure the beam polarization, is a crucial item for the success of the RHIC spin program. We consider an asymmetry A_N in inclusive pion production by polarized protons as a possible base for the RHIC polarimetry.

At high energy, single transverse spin asymmetries have been expected to be small. However, the Fermilab E704 experiment [1] showed significant spin effects in the reactions $p_\uparrow p \to \pi^+ X$ and $p_\uparrow p \to \pi^- X$ at 200 GeV. A striking dependence on Feynman x was observed in which A_N increased from 0 to about 0.3 with increasing x_F for the π^+ data and decreased from 0 to about -0.3 with increasing x_F for the π^- data. The results on A_N for the E704 experiment are presented in Fig.1.

Besides pion asymmetries, large effects were observed for the transverse polarization P_N of inclusive hyperons from unpolarized beams and targets [2]. In hyperon production, the magnitude of the polarization seems to be insensitive to energy over fixed target energies from 12 GeV to 2000 GeV, and it is only slightly smaller for nuclear targets compared to hydrogen, which is explainable as a rescattering effect [2]. There is a reason to believe that the asymmetries in meson and the polarization in hyperon production are related [3,4]. Therefore, based on the E704 results, we can expect big asymmetries in pion inclusive production in the whole polarized RHIC energy range, from 23 to 250 GeV.

In this paper we present the results of the measurements of the asymmetries in the inclusive reactions:

$$p_\uparrow C \to \pi^+ X, \tag{1}$$

$$p_\uparrow C \to \pi^- X, \tag{2}$$

$$p_\uparrow C \to p X. \tag{3}$$

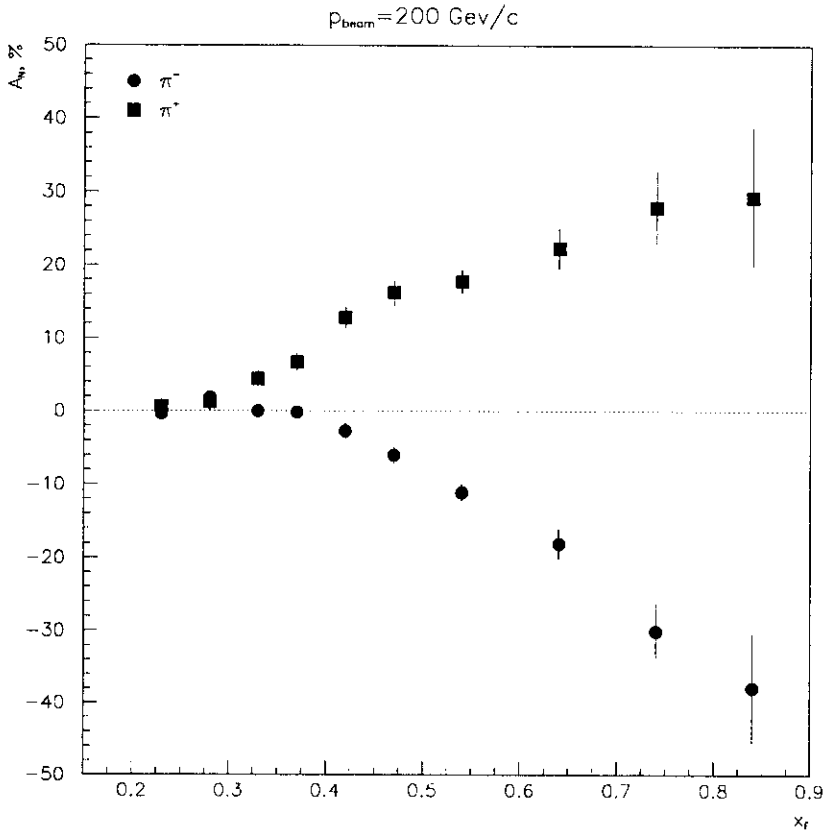

Fig. 1. Asymmetry A_N versus x_F for π^+ and π^- data in the E704 experiment at Fermilab. The incident momentum of the polarized proton beam is 200 GeV/c, and p_T−region is from 0.2 to 2.0 GeV/c.

A transversely polarized 21.6 GeV/c beam in an extracted beam line from the Brookhaven Alternating Gradient Synchrotron (AGS), and a carbon target have been used. The kinematic range covered by the experiment was transverse momentum p_T from 0.3 to 1.2 GeV/c, and $x_F = p_L{}^*/P_{max}{}^*$ from 0.45 to 0.8. The data were taken in November 1997. The main purpose of the experiment was to obtain basic information in order to design a polarimeter for the RHIC polarized beams. The use of a carbon target instead of a hydrogen one (as in E704) would be much cheaper for the RHIC polarimeter. Through this experiment we were able to test both the energy and target dependence of inclusive pion production by comparing our results with the 200 GeV data and with some low energy data as well.

2. POLARIZED BEAM AND POLARIMETER

The polarization of the beam, obtained from the asymmetry of pp elastic scattering (polarimeter for E925), and the asymmetry of an inclusive process were measured simultaneously. Two sets of counters, electronics, and data acquisition systems were used. These side-by-side experiments were triggered separately and the data were accumulated separately. The experimental layout is sketched in Fig.2.

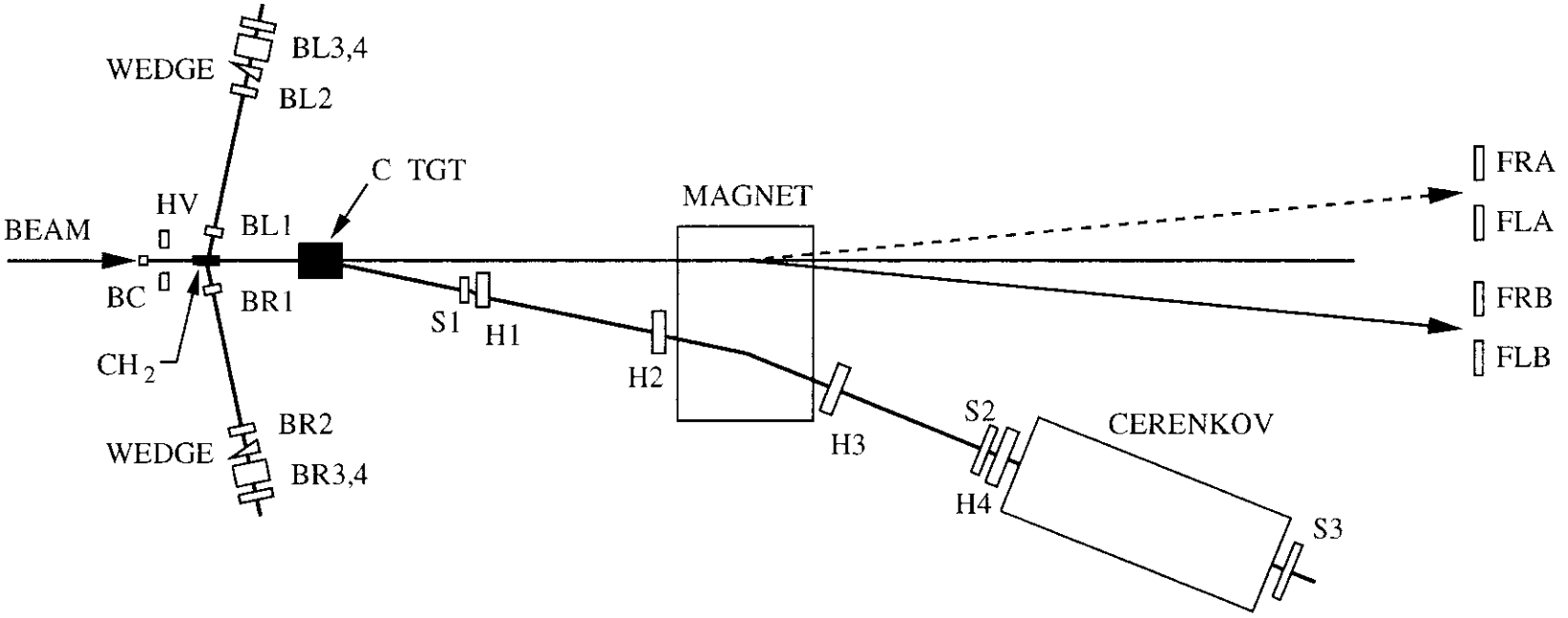

Fig. 2. Scheme (not to scale) of the experemental setup showing the C and CH_2 target, analysing magnet, and particle detectors, as described in the text.

The beam, 3×10^7 per AGS cycle, was transversely polarized in the vertical direction, perpendicular to the horisontal scattering plane. The polarization direction was flipped each pulse to reduce systematic errors. The beam was debunched, and extracted with a 0.5 sec flattop at 2.5 sec per cycle.

The main task of the elastic arm was to obtain the absolute value of the polarization of the proton beam extracted to the B1 beam line. The analyzing power A_N of the elastic *pp*-scattering at t=-0.15 $(\mathrm{GeV/c})^2$ is known within 10%, therefore the beam polarization can be determined from the asymmetry of the elastic *pp*-scattering.

2.1. Experimental Setup for Elastic *pp*-scattering

The kinematic region of interest for the *pp*-scattering was around $-t = 0.15 \pm 0.05\ (\mathrm{GeV/c})^2$. According to the previous measurements [6], this range gives the largest asymmetry. Fig.3 shows the kinematic variables in this region for the initial proton momentum 23 GeV/c. We planned to detect both the recoil protons and the forward protons. In order to accept all of them, the backward counters should cover the angle from 76 to 80° and the forward ones should cover the angle from 0.80 to 1.12°.

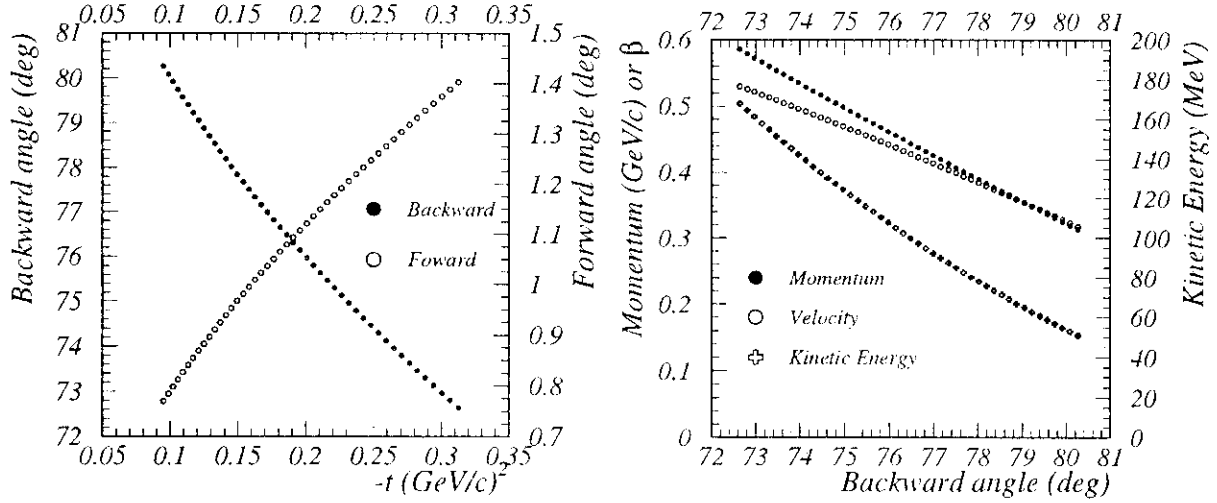

Fig. 3. Kinematics of the elastic *pp*-scattering at 23 GeV/c. The angle is defined with respect to the beam axis.

The elastic detector was a double arm telescope (Fig.2). Each arm consisted of four backward (B1, B2, B3, B4) and two forward counters (F). Each counter consisted of a plastic scintillator and one or two photomultiplier tubes (PMT) (Hamamatsu H1161-50). The size of scintillators and their positions are summarized in Table 1. The B1 determined the trigger timing. The signal of B2 was read from both sides by PMT and was named as B2U (up-) and B2D (downstream). The time difference between B1 and B2 gave the Time-Of-Flight (TOF) information. As is clear from Fig.3, the backward proton velocity was within the range $\beta = 0.32 \sim 0.45$, which corresponds to the time of flight from 9.8 to 7.0 nsec, whereas $\beta = 1$ corresponds to 3.1 nsec. For the TOF to be useful, it was necessary to have a resolution of 1 nsec.

Table 1. The counters positions and dimensions.

Name	size $[h \times w \times t]$ (mm^3)	position from the target
B1	$20 \times 15 \times 1$	8 cm, 78°
B2	$70 \times 80 \times 2$	102 cm, 78°
B3	$70 \times 80 \times 45$	114 cm, 78°
B4	$80 \times 100 \times 10$	116 cm, 78°
F	$10 \times 60 \times 10$	~11 m, ~ 0.96°

There were aluminum absorbers of a wedge shape between B2 and B3 in both arms. As one can see from Fig.3, the kinetic energy of the recoil protons is a function of the scattering angle. The wedge was supposed to equalize the recoil protons kinetic energy. The scintillators B3 were thick enough to absorb the recoil protons. The particles that passed through B3 and reached B4 were probably pions and were, therefore, vetoed.

The forward counters detected the forward protons and selected the elastic events by the coincidence with the B counters. Since there was a π analyzing magnet before the F counters, these counters must be placed so that to account for the effect of the magnetic field. For B-polarity positive charged particles bended to the π arm direction (the right direction if we look downstream). The A-polarity was set for the π^- detection. The forward counters were named as follows: FRA, FLA, FRB and FLB. L or R marks the direction to the right or to the left of backward arms. The standard momentum kick of the analyzing magnet was 1.0 GeV/c, which corresponds to 1725 A at p_{lab} =21.6 GeV/c. When the beam intensity was too high for the operation of the beam counter BC, we did not use it at all.

High voltage for each counters was set so that a typical pulse height was equal to ~ 100 mV (about 1050 V for B3 and higher (up to 1640 V) for the others). The discriminator threshold for all the counters was 40 mV. The B3 scintillator was the Bicron #400 and the B124 and F one was #408.

The TDC and ADC of all the counters (B1234, F, BC) were recorded (except ADC of BC). The TDC full scale was 200 nsec and 10 channels corresponded to 1 *nsec*. Single counts, coincidence counts, halo veto (HV) and luminosity monitor counts were read by the CAMAC scalers.

Since it was suspected that HV eliminated some useful events, we carried out the run without it. In addition, we wanted to monitor the asymmetry by the backward arm only and we did not include F counter in the trigger. A typical trigger was as follows: $\left[(BL1 \otimes BL2U \otimes BL2D \otimes BL3 \otimes \overline{BL4}) \oplus (BR1 \otimes BR2U \otimes BR2D \otimes BR3 \otimes \overline{BR4})\right]$. The target for the elastic experiment was polyethylene (CH_2) and had dimensions $5 \times 30 \times 15$ mm^3. In order to estimate a carbon contamination from CH_2, we used a carbon target which had dimensions $2 \times 30 \times 15$ mm^3.

2.2. Data Analysis and Results

We have measured the asymmetries at the beam momentum p_{lab} =21.6 GeV/c. The runs have been grouped in three periods, P1, P2 and P3. We changed the target twice and carried out the set of carbon-empty target runs. First of them was between periods P1 and P2, and the other was after P3. It was realized that the beam was shifted from the target center (3-4 mm) until the end of P2. The P3 period started after we had corrected this. We also reversed the analyzing magnet polarity time-to-time. Combining these periods and the analyzing magnet polarity, we classified five periods as P1A, P1B, P2B, P3B and P3A.

It was most important to know the polarization when the pion inclusive data were collected. To satisfy this condition, we analyzed only those data sets, that had both the pion and elastic data.

The information on an absolute beam intensity was necessary to extract the cross sections, and the relative intensity monitor was needed to compare the data from different targets. The beam intensity was monitored with two luminosity telescopes, consisting of three scintillators each, placed at $\pm 16°$ in the vertical plane defined by the beam momentum and polarization vectors (downstream the carbon target). This angle with respect to the beam momentum placed these telescopes at $\sim 90°$ in the center of mass (c.m.) frame. These two facts were combined to minimize any possible polarization effects in the beam normalization. The LOR monitor (the number of counts when there was a signal from the coupled up or down scintillators) was used for the inclusive asymmetries measurement. An ionization chamber was also used to monitor beam intensity.

A "hit" was determined in the following procedure:

1. Selection of events whose TDCs were not overflowing (pre-TDC cut). The ADC and TDC spectra after this step are plotted in Fig.4 and Fig.5 (black lines).
2. ADC cuts for each counter were applied. Each threshold was chosen so that it slightly cuts the signal region. Spectra after these cuts are shown in gray.
3. TDC (or TOF) spectra were fitted by Gaussian, the events selected within $n \cdot \sigma$ range ($n = 1, 2, 3$). (The final TDC cut).

For the forward TDCs and backward TOFs, various cuts (1, 2 and 3 σ) were examined. The 2 or 3 σ cuts do not show any significant difference. We will present the results with 2σ cut later on. (Fig.4 and 5 show the case of 2σ cut).

Comparing an empty target run or a carbon target run with the CH_2 target runs, one can estimate the background emerging not from the target region or a fraction of events originating from the carbon. The results are given below.

- Carbon contribution to Backward arm: about 50% (40-60%)
- Carbon contribution to coincidence: 2-4%
- Non-target contamination of particle to Backward arm: 1-5%
- Non-target contamination of particle to coincidence: negligible ($< 0.3\%$).

Raw asymmetries ϵ have been calculated by

$$\epsilon \equiv \frac{\sqrt{N_L^{\uparrow} \times N_R^{\downarrow}} - \sqrt{N_L^{\downarrow} \times N_R^{\uparrow}}}{\sqrt{N_L^{\uparrow} \times N_R^{\downarrow}} + \sqrt{N_L^{\downarrow} \times N_R^{\uparrow}}}, \tag{4}$$

where N_L (N_R) is the number of counts detected in the left (right) arm. Superscript $^{\uparrow}$ ($^{\downarrow}$) indicates that the polarization is up (down). Its statistical error is given by the following formula:

$$\delta\epsilon = \frac{1}{L+R}\left(\frac{LR}{L+R}\right) \times \sqrt{\frac{1}{N_L^{\uparrow}} + \frac{1}{N_R^{\downarrow}} + \frac{1}{N_R^{\uparrow}} + \frac{1}{N_L^{\downarrow}}}, \tag{5}$$

where $L \equiv \sqrt{N_L^{\uparrow} \times N_R^{\downarrow}}$ and $R \equiv \sqrt{N_L^{\downarrow} \times N_R^{\uparrow}}$.

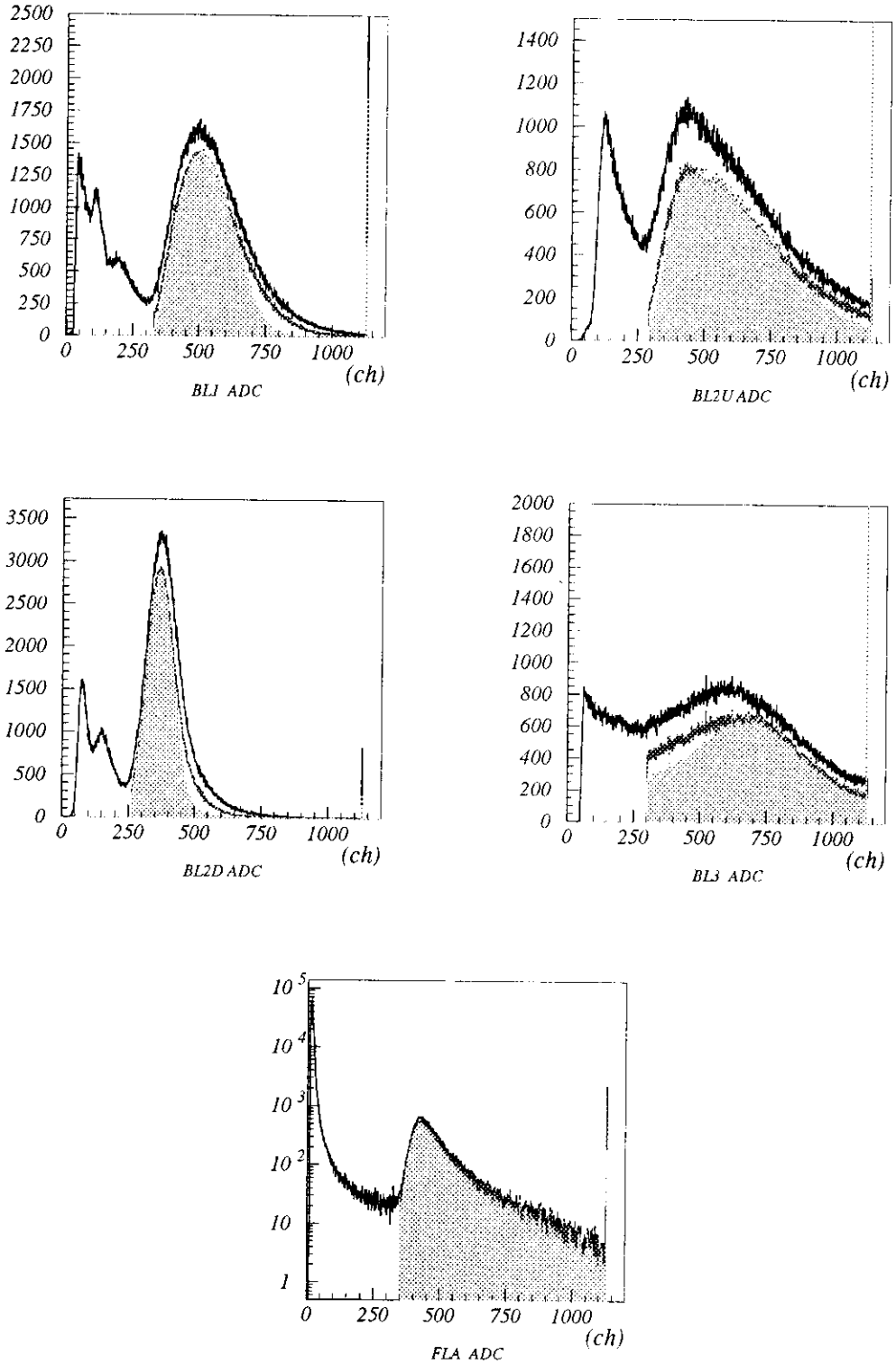

Fig. 4. ADC cut examples. Black line is pre-TDC cuts. For backward counters, gray line is after ADC cuts, and hatched region indicates after final TDC cut.

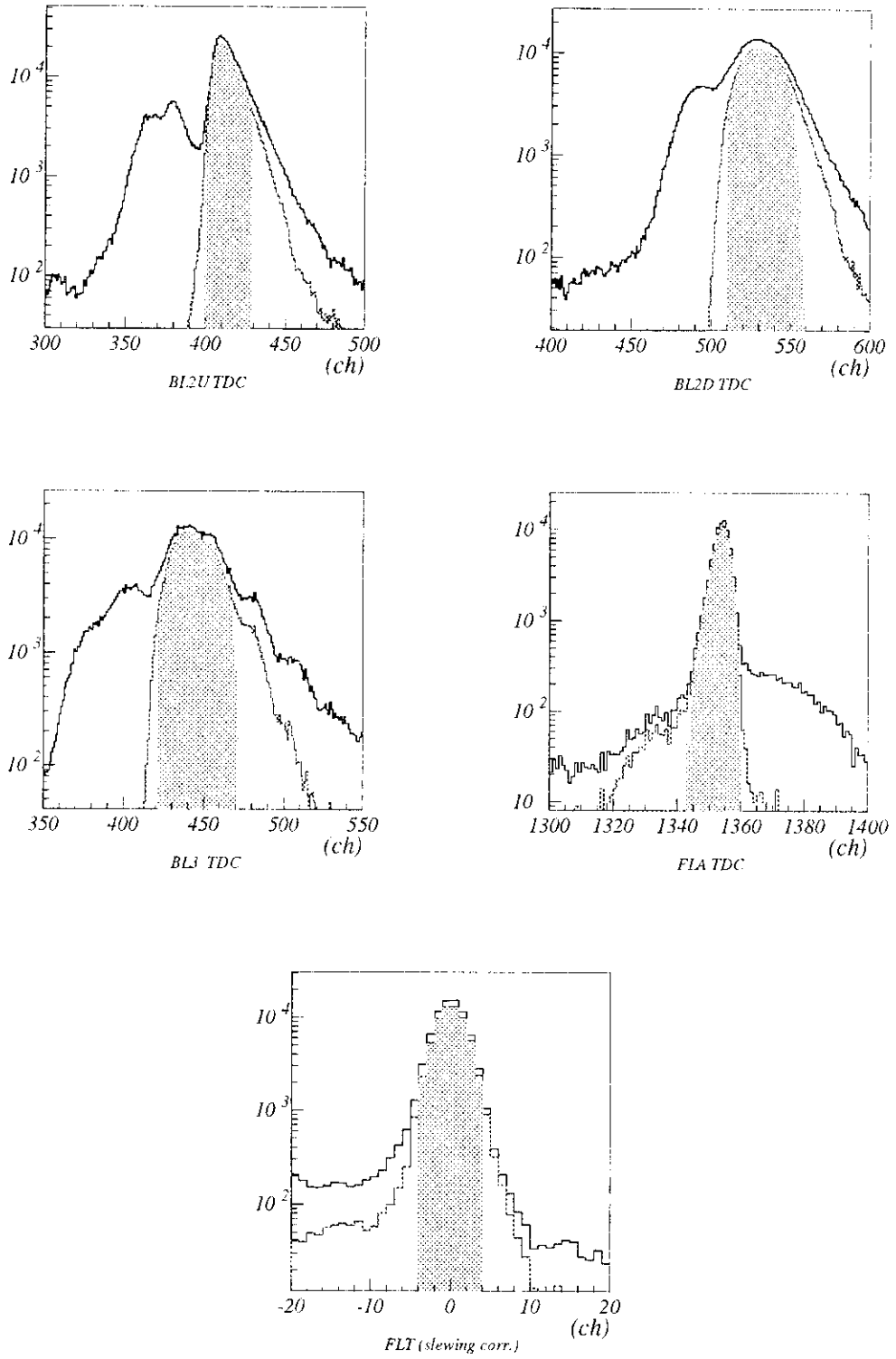

Fig. 5. TDC cut examples. Lines color-code are the same as the previous one. The last two figures are for a one of forward counters (before and after slewing correction). Gray line is after forward ADC cut and hatched region remains after final cut.

There is a simple relation ($\epsilon = P_B\ A_N$) among ϵ, the beam polarization P_B, and the analyzing power A_N. For this relation to be exact, the counter acceptance and efficiency should be constant in time, the absolute polarization value of both signs has to be equal, and no scattering angle dependence should be on the analyzing power. Since we flipped the polarization sign every burst, the counter acceptance and efficiency were constant. It would be reasonable to assume that the absolute polarization values for both signs were equal.

The results of raw asymmetries are presented in Table 2 for five different periods, total average and carbon one. They have been extracted from the back-forward coincidence events. Table 3 is similar but with using backward arms only, which has much more statistics. The comparison of the raw asymmetry with E880 data (internal polarimeter) shows a good agreement. But there was not enough carbon data and the systematic uncertainties were not estimated. Therefore, we did not use these data to extract the absolute value of the polarization. The final physical raw asymmetry of CH_2 (ϵ_{CH_2}) have been determined as

$$\epsilon_{CH_2} = 0.0107 \pm 0.0023. \tag{6}$$

Table 2. Physical and false asymmetries for each period with the 2σ TDC cut with $B \times F$ coincidence. Notice that the sign is opposite to the conventional definition written in the text.

Period	ϵ	$\alpha_{11} \simeq \epsilon_B$	$\alpha_{10} \simeq \epsilon_\Omega$
P1A	-0.0152 ± 0.0119	-0.0152 ± 0.0119	-0.1799 ± 0.0115
P1B	-0.0224 ± 0.0063	-0.0077 ± 0.0063	-0.2240 ± 0.0060
P2B	-0.0112 ± 0.0052	0.0092 ± 0.0052	-0.1820 ± 0.0051
P3B	-0.0110 ± 0.0129	-0.0195 ± 0.0129	-0.0505 ± 0.0128
P3A	-0.0076 ± 0.0029	0.0001 ± 0.0029	-0.0238 ± 0.0029
Total	-0.0107 ± 0.0023	0.0000 ± 0.0023	-0.0878 ± 0.0022
Carbon	-0.0841 ± 0.0449	-0.0643 ± 0.0450	-0.0195 ± 0.0452

Table 3. The same as in the previous table, but the data with Backward arm only.

Period	ϵ	$\alpha_{11} \simeq \epsilon_B$	$\alpha_{10} \simeq \epsilon_\Omega$
P1A	-0.0121 ± 0.0050	0.0035 ± 0.0050	-0.1043 ± 0.0049
P1B	-0.0111 ± 0.0025	-0.0044 ± 0.0025	-0.1094 ± 0.0025
P2B	-0.0081 ± 0.0020	0.0019 ± 0.0020	-0.0945 ± 0.0020
P3B	-0.0095 ± 0.0051	-0.0067 ± 0.0051	-0.0392 ± 0.0051
P3A	-0.0090 ± 0.0012	0.0008 ± 0.0012	-0.0467 ± 0.0012
Total	-0.0092 ± 0.0009	0.0002 ± 0.0009	-0.0667 ± 0.0009
Carbon	-0.0030 ± 0.0052	-0.0080 ± 0.0052	-0.0205 ± 0.0052

Two kinds of a false asymmetry are also shown in the tables. Beam asymmetries (ϵ_B) were small for the most of runs (less than 0.02 for all CH_2 runs). Detector asymmetries (ϵ_Ω) varied and were large (up to 0.20) for period P1A, P1B and P2B. But it is understandable, because the beam position was not stable. (Numerical values shown in Tables 2, 3 are α_{10} or α_{11}. They are approximately equal to ϵ_B or ϵ_Ω (see Appendix)).

In principle, carbon contribution should be subtracted from ϵ_{CH_2} in order to extract the asymmetry ϵ_p of elastic pp-scattering. However, the statistics of the carbon data is not enough to correct the ϵ_{CH_2}. The measured carbon data were not used because:

- Statistics is small. The measured asymmetry (ϵ_C) do not differ more than 2σ from zero.
- No data have been taken for B-polarity.
- E880 data or our backward data do not show any indication that the carbon asymmetry is large.
- No data available at this energy, but A_C is smaller than A_p at $p_{lab} = 3.5$ GeV/c [9] and at $p_{lab} = 185$ GeV/c [10].

Therefore, we examined two cases:

1. $A_C = A_{CH_2}$ or
2. $A_C = 0$.

We obtained ϵ_p as

$$\epsilon_p = \frac{\epsilon_{CH_2} - n_c \times \epsilon_C}{n_p}, \tag{7}$$

where n_p is the elastic pp ratio in the CH_2 target and n_C is the fraction of the carbon in the CH_2 target. It was supposed that $n_p + n_C \equiv 1$. The error is given by

$$(\Delta\epsilon_p)^2 = (\frac{\Delta\epsilon_{CH_2}}{n_p})^2 + (\epsilon_C - \epsilon_{CH_2})^2(\frac{\Delta n_p}{n_p^2})^2 + (1 - \frac{1}{n_p}\Delta\epsilon_C)^2. \tag{8}$$

Using $n_p = 0.97 \pm 0.01$ we obtained the numerical results as follows:

- $A_C = A_{CH_2}$: $\epsilon_p = 0.0107 \pm 0.0023$
- $A_C = 0$: $\epsilon_p = 0.0110 \pm 0.0026$

For the final result, we took their mean value:

$$\epsilon_p = 0.0108 \pm 0.0024(stat.) \pm 0.003(syst.). \tag{9}$$

The statistical error (stat.) comes from the first term of equation (8). The systematic error (syst.) comes from the sum of the second and the third term of equation (8). The systematic error depends on the A_C value.

In order to obtain the polarization, we used the analyzing power $A_N = 0.040 \pm 0.004$ at p_{lab} =21 GeV/c and $t = -0.15$ (GeV/c)^2. This value was determined from a phenomenological analysis of existing data [6,7,8]. It gave the beam polarization as follows:

$$P_B = 0.271 \pm 0.059(stat.) \pm 0.028(syst.). \tag{10}$$

Appendix

The following quantities (α_{10} and α_{11}) are defined in [5]. They are approximately equal to the counter acceptance asymmetry and the beam (intensity) asymmetry.

$$\begin{aligned} \alpha_{10} &\equiv \frac{\sqrt{N_L^\uparrow \times N_L^\downarrow} - \sqrt{N_L^\downarrow \times N_L^\uparrow}}{\sqrt{N_R^\uparrow \times N_R^\downarrow} + \sqrt{N_R^\downarrow \times N_R^\uparrow}} \\ &= \epsilon_\Omega + \frac{pA}{1 - p^2A^2}\epsilon_p - \frac{p^2A^2}{1 - p^2A^2}\epsilon_A + \mathcal{O}(\epsilon^3) \\ &\simeq \epsilon_\Omega \end{aligned} \tag{11}$$

$$\begin{aligned} \alpha_{11} &\equiv \frac{\sqrt{N_L^{\uparrow} \times N_R^{\uparrow}} - \sqrt{N_L^{\downarrow} \times N_R^{\downarrow}}}{\sqrt{N_L^{\uparrow} \times N_R^{\uparrow}} + \sqrt{N_L^{\downarrow} \times N_R^{\downarrow}}} \\ &= \epsilon_B + \frac{pA}{1 - p^2A^2}\epsilon_A - \frac{p^2A^2}{1 - p^2A^2}\epsilon_p + \mathcal{O}(\epsilon^3) \\ &\simeq \epsilon_B \end{aligned} \tag{12}$$

- ϵ_Ω: the left-right asymmetry of the polarimeter acceptance or solid angle
- ϵ_A: the left-right asymmetry of the calibration constant
- ϵ_B: the asymmetry of the beam intensity for spills with beam polarization up and down
- ϵ_p: the asymmetry of the beam polarization for spills with beam polarization up and down.

3. EXPERIMENTAL TECHNIQUE FOR INCLUSIVE ASYMMETRIES MEASUREMENT

An entirely separate set of counters, H1–4, S1–3, and a threshold Cherenkov counter, were used to measure the asymmetry of inclusive pion production (see Fig.2). The transversely-polarized proton beam impinged upon a 4.0 cm thick carbon target. The x-positions (the horizontal coordinate) of charged particles emerging from the target were measured before and after the analyzing magnet in the hodoscopes H1 and H2 (each consisted of 31 cells of 2 mm wide), H3 (47 cells of 2 mm wide), and H4 (55 cells of 2 mm wide). These last two hodoscopes also measured the vertical position of the particle tracks. Each of these hodoscopes consisted of 6 mm wide scintillators with 1/3 overlap. The magnetic field provided a p_T-kick of around 1 GeV/c and could be reversed to select the charge of the inclusive particles. The x-positions from these four hodoscopes provided for the measurement of the production and bend angles, and hence also the momentum, x_F, and p_T. The trigger consisted of a coincidence among scintillators S1, S2, and S3, and hits in 3 out of 4 hodoscope x-planes in H1–4. The halo veto scintillator was used to better define the beam spot and caused an electronic veto of events. The 1.6 m long Cherenkov counter, filled with CO_2 at a pressure of $\sim$ 2 atmospheres, allowed the differentiation between pions and protons. For π^+, the Cherenkov counter was required in the trigger to eliminate a large flux of protons, except for the runs to measure the proton production analyzing power.

The Cherenkov counter threshold was set to give an efficiency $> 95\%$ for a 3 GeV/c pion beam. In the x_F and p_T region of this experiment, the efficiency for pions was estimated to be 98%, and the contamination of protons in the π^+ data is expected to make a negligible change to the analyzing power. Based on the measured cross sections for $p + Be$ interactions at 24 GeV/c [12], there could be a $20 - 25\%$ contamination of K^+ in the raw π^+ data. It is estimated that this was reduced to below 3% by a pulse height requirement on the Cherenkov counter. For the π^- results, the contamination by K^- is expected to be less than 3% and by antiprotons to be negligible [12].

4. DATA ANALYSIS AND RESULTS

4.1. Selection of Events

The data were collected and written to a disc at incident momenta 21.6 GeV/c and two polarities of the analyzing magnet. The number of events recorded for the analyzing magnet set

in one polarity, where negatives were deflected to the right, was about 2.0×10^6 with 20% of these reconstructed events. When the analyzing magnet was set in the opposite polarity (positives deflected to the right), approximately 4.0×10^5 inclusive proton and 2.5×10^6 inclusive π^+ triggers were recorded, with 67% and 48% reconstructed events, respectively. These relatively low numbers of the reconstructed events were due to trigger conditions rather than due to a software reconstruction efficiency, which was about 95% for $SX_{min} < 0.05$ cm^2 [11].

4.1.1. Event reconstruction

The reconstruction procedure [11] has been provided as follows. After an event decoding, the analyzing program was looking for clusters in each plane of the hodoscopes. The cluster was defined as a group of adjacent cells hitted. For each possible combination of clusters in X-planes of the four hodoscopes, a fit was made to determine three track parameters, AX, BX, and P. AX and BX were an angle and an x-coordinate of the track projected back to the target, and P was a momentum associated with the track. An x-coordinate of the track at any z-pozition between the target and the analyzing magnet was defined as $x = AX \times z + BX$. A parameter SX, a type of χ^2, was determined to compare the hits in four X-planes of the hodoscopes with iterative values of the reconstructed track. The SX was defined as

$$\sum_{i=1}^{4}(x_i - f_i)^2,$$

where x_i was the center of the cluster in the i-th hodoscope, and f_i was the value of the fitting function for the i-th hodoscope, that took into account a magnetic field magnitude in the analyzing magnet. If a combination of four clusters in four X-planes of the hodoscopes with a minimal SX_{min} satisfied the condition $SX_{min} < 0.32$ cm^2, the event was considered as a reconstructed one and was stored for a further analysis.

An influence of a noise in the hodoscopes on a reconstruction efficiency and on x_F-resolution was studied. Noise characteristics of the hodoscopes were extracted from the experimental data. In the reconstructed events, clusters on a track were crossed out, and the four distributions of the rest hits in the four hodoscope X-planes were accumulated. They turned out to be flat. The noise characteristic was defined as a probability besides a track cluster to find in the same event a noise cluster, which could come either from a particle, which emerged from the interaction point and hitted the hodoscope or from a hodoscope noise itself. This value decreased from 15% for the first hodoscope down to 5% for the last one.

GEANT Monte Carlo calculations were made to understand the dependence of the reconstruction procedure on a background. The noise numbers in all the hodoscopes were stable within 10% (relative deviations) during the data taking time. As a result, the reconstruction efficiency was almost the same during this period. The x_F-resolution was about 0.01 and depended on a noise increase weakly. The p_T-resolution depended on p_T weakly and its value was about 0.02 GeV/c.

4.1.2. Criteria applied to select good events

All the reconstructed events were broken into the runs. Each run corresponded to a beam time around one hour, in average. In order for the run to be included in the data sample for analysis, it had to pass some software requirment. The ratios of the LOR monitors for two beam polarization signs for each run were calculated. Only the runs with a ratio close to 1 were selected for the further analysis.

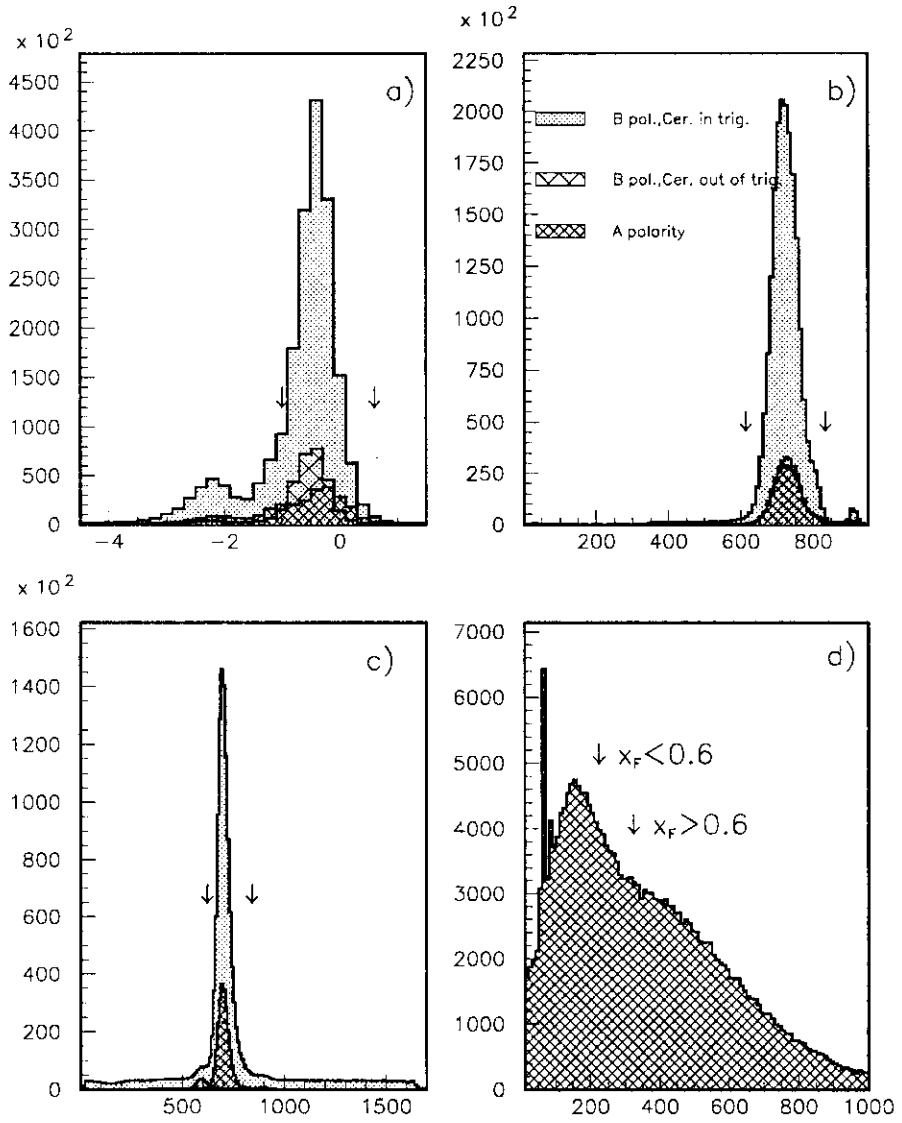

Fig. 6. a) Distributions of $x-$coordinate of a track at the target (BX); b) distributions of a time of particle flight between S1 and S3 (TDC2); c) distributions of a time of particle flight between S1 and the Cherenkov counter (TDC1); d) a distribution of ADC amplitude from the Cherenkov counter. For π^- the analyzing magnet polarity was A, and for π^+ it was B. When the Cherenkov counter was in trigger, π^+ were selected and protons were rejected at the trigger level. The selected areas for good events are indicated by arrows.

For the reconstructed events, a BX-distribution (x-coordinate of a track at $z = 0$, that was the center of the target) was accumulated (see Fig.6a), where the events with chosen BX-values from -1.0 to 0.6 cm were supposed to be produced at the target.

For each event, there was a TDC2 value. It stood for a time-digital-convertor signal which corresponded to the time of a particle flight between the scintillator counters S1 and S3. A signal from S1 was used as a start signal for TDC2, and a signal from S3 as a stop signal. The TDC2 distribution is presented in Fig.6b. The selected area was between 620 and 840. So, a particle had to have both a valid x-coordinate value at the target and the time of flight between S1 and S3. These two first criteria applied to select good events were the same for all three

reactions with π^+, π^-, and protons in the final state. The next two criteria were connected with the Cherenkov counter, which had to kill proton and kaon contaminance in the π^+ sample, and distinguish protons from pions. For π^- mesons, a contaminance of K^- was expected at the level of 3% and less, and a $\bar{p}$ contaminance was negligible. That is why the Cherenkov counter information has not been used for π^- analysis. So, for π^-mesons the above two criteria were the only ones.

There were two signals from the Cherenkov counter. The first one was a TDC1 signal (see Fig.6c), which measured the flight time of a particle between the S1 and the back plane of the Cherenkov counter. The selected area for pions was between 640 and 840. For protons the TDC1 value had to be greater than 2000. There was no stop signal for protons, and the 11-bit TDC electronic module was saturated.

The second signal from the Cherenkov counter was an ADC amplitude which was proportional to the Cherenkov light intensity. The threshold curve of the Cherenkov counter was obtained from a special run with low value of magnetic field in the analyzing magnet. Pions from a momentum of 3 GeV/c and higher were detected with a maximal efficiency, which was about 95%. This means that kaons with a momentum of 12 GeV/c ($x_F = 0.55$) and higher were also detected by the Cherenkov counter with the same efficiency. Protons had to be detected at $x_F > 0.95$. The ADC spectrum for π^- (A-polarity of the analyzing magnet) is presented in Fig.6d.

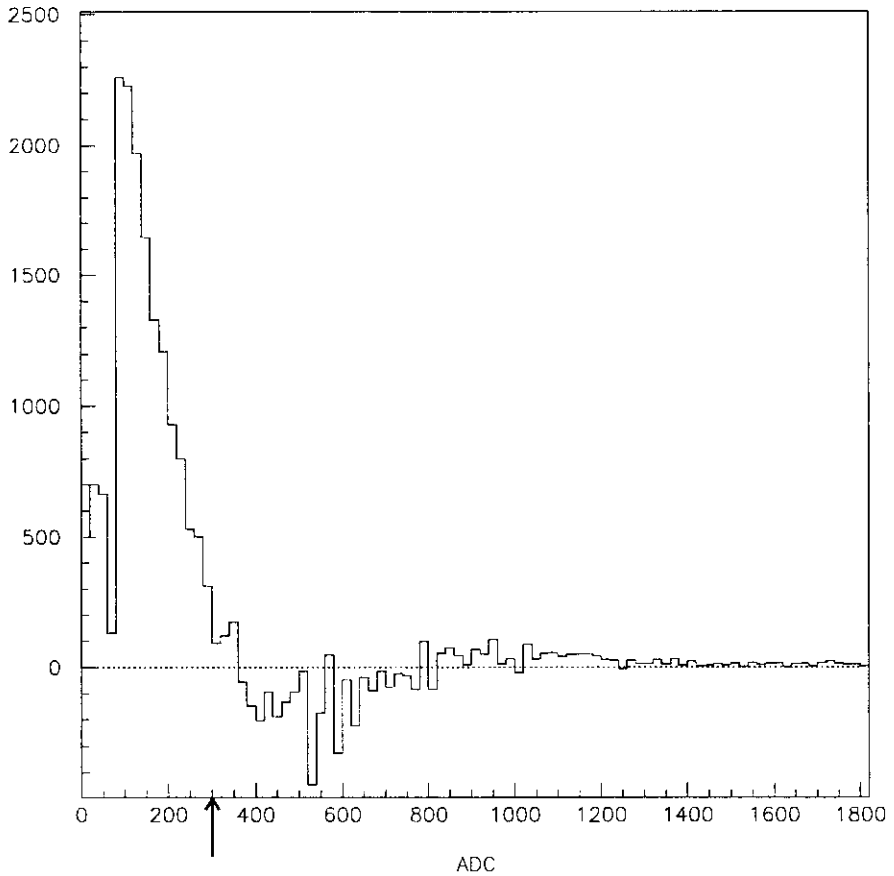

Fig. 7. The ADC spectrum of K^+-mesons as a difference between π^+ (including K^+) and π^- spectra.

As is known [12], the K^+-contamination to pions grows with a x_F increase and reaches a value of about 30% at $x_F = 0.75$. We extracted the ADC spectrum of K^+-mesons by subtracting the π^--spectrum from π^+ after they had been normalized to one on other in the region $ADC > 400$, where there was practically no K^+-contamination to the π^+ data. A typical spectrum of K^+

is shown in Fig.7. The arrow points to the ADC cut, which should be applied to suppress kaons. The cuts were as follows: no ADC cut at $x_F < 0.55$, $ADC > 200$ at $0.55 < x_F < 0.6$ and $ADC > 300$ at $x_F > 0.6$. We estimated the K^+-contamination remained after the proper ADC cuts had been applied as less than 2%, at least. To select protons, the ADC value had to be less than 70.

A SX_{min} distribution for the reconstructed events had a sharp peak near zero and a long tail. The sharp peak corresponded mainly to real particles which went through all four hodoscopes. The tail consisted mainly of a background from accidental coincidences in the hodoscopes. Simulation [11] has shown that 95% of the real events were in the region with $SX_{min} < 0.05\ cm^2$. Only 0.1% of the real events turned out to be in the region with $SX_{min} > 0.32\ cm^2$. The SX_{min} distributions depended strongly on x_F. A background tail increased significantly relative to the peak value with x_F increased. The SX_{min} distributions for different x_F-bins for π^- mesons, where the relative background was the biggest due to low π^- cross section, are presented in Fig.8. The region $SX_{min} < 0.05\ cm^2$ was selected to calculate asymmetries and cross sections.

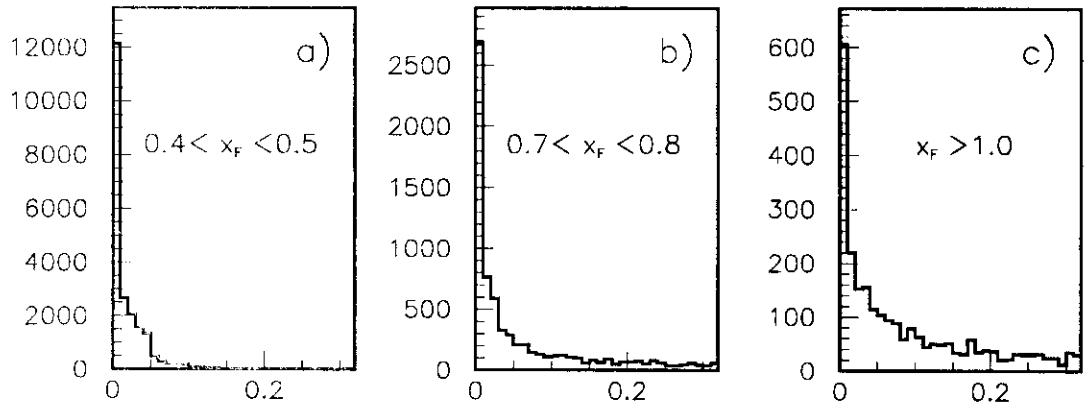

Fig. 8. The SX_{min} distributions for the π^- mesons at different x_F−regions: a) $0.4 < x_F < 0.5$; b) $0.7 < x_F < 0.8$; c) $1.0 < x_F < 1.1$.

The distribution of accepted events in x_F and p_T is shown in Fig.9.The inclusive charged particle production measurements started at x_F around 0.4 and p_T around 0.3 GeV/c due to the set-up acceptance. A beam running time allowed us to reach x_F around 0.8 and p_T about 1.2 GeV/c. The proper cuts were applied.

Eventually, the numbers of the events that survived every software requirment mentioned above for π^-, π^+, and protons are included in Table 4.

Table 4. The numbers of events surviving after applying miscellaneous software cuts. Details are in the text.

criterium	π^-	π^+	protons
1. total number of reconstructed events	408,883	1,188,308*	269,634*
2. bad LOR ratio	399,634	1,179,679	—
3. BX (x-coordinate at target)	271,009	889,666	237,980
4. TDC2 (S1 to S3)	257,082	836,895	231,405
5. TDC1 (S1 to Cherenkov)	—	605,406	214,502
6. ADC on Cherenkov	—	448,232	—
7. $SX_{min} < 0.05$ cm^2	225,939	404,469	199,757
8. $0.45 < x_F < 0.8$ and 0.3 GeV/c$< p_T <$1.2 GeV/c	218,868	399,024	192,359

* protons were selected by $ADC < 70$ applied cut already at the level 1 of table 4. No additional ADC cut was applied for the protons. Also at the same level only those events were accounted as π^+−mesons, which survived a cut $ADC > 70$.

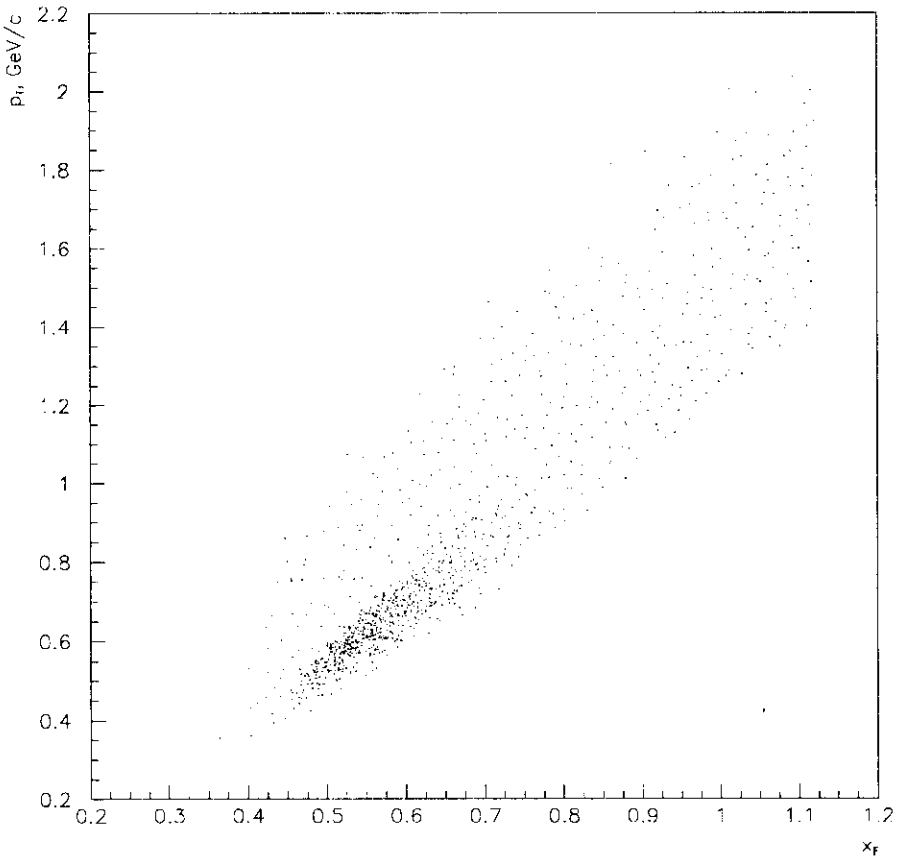

Fig. 9. Scatter plot of $x_F - p_T$ reconstructed π^-, π^+, and proton events survived after applying all constraints.

4.1.3. Background estimate

To estimate the background, the ratios of the number of events in the region $SX_{min} < 0.05$ cm^2 to the number of events in the tail region $0.16 < SX_{min} < 0.32$ cm^2 were defined for π^+, π^-, and protons by using SX_{min} distributions in the kinematically forbidden region $1.0 < x_F < 1.1$, which consisted of the background events only. We should mention, that both SX_{min} distributions at $x_F < 0.8$ (the region of interest) and $x_F > 1.0$ had the same shape, namely, a sharp peak near zero and a long tail (see Fig.8). For π^- the forbidden region was extended to $x_F = 0.85$, because there are practically no π^- above this x_F value. The results are presented in Table 5.

Table 5. The ratios of the number of the events in the region $SX_{min} < 0.05$ cm^2 to the number of the events in the tail region $0.16 < SX_{min} < 0.32$ cm^2

reaction	kinematically forbidden region	ratio
π^-	$0.85 < x_F < 0.92$	2.41 ± 0.13
π^-	$0.92 < x_F < 1.00$	2.49 ± 0.16
π^-	$1.00 < x_F < 1.10$	2.56 ± 0.18
π^+	$0.92 < x_F < 1.00$	2.47 ± 0.21
π^+	$1.00 < x_F < 1.10$	2.30 ± 0.23
average ratio		2.45 ± 0.08

The ratios were the same within the errors. The background, which was calculated by using experimental data, did not depend on the sort of particles and on the x_F in the region $0.85 < x_F < 1.1$, and was the same for both signs of the beam polarization. The average value of the ratio was found to be $r = 2.45 \pm 0.08$. We could not check directly whether the background shape in the region of interest, $0.45 < x_F < 0.8$ and $0.4 < p_T < 1.2$ GeV/c, obeyed the same ratio, because there was a contamination of real inclusive and background events in this region. Based on the study of pure background experimental data, we assumed that the background shape did not depend on x_F in the whole region of interest. The ratio r was used for the background estimate for π^+, π^-, and protons at any x_F and any p_T. The ratio r is slightly smaller than the one for protons in the kinematicaly forbidden region, which was 3.22 ± 0.45, but as we can see from Table 6 the background for protons is pretty small. We estimated the systematic error by using different tail regions in the background calculation as 9% for pions and 32% for protons.

Table 6. Background in the region $SX_{min} < 0.05$ cm^2. Details are in the text.

$< x_F >$	π^-	π^+	protons
0.48	0.034 ± 0.002	0.035 ± 0.002	0.015 ± 0.002
0.53	0.040 ± 0.002	0.033 ± 0.001	0.020 ± 0.001
0.57	0.052 ± 0.002	0.043 ± 0.002	0.024 ± 0.001
0.62	0.089 ± 0.004	0.056 ± 0.002	0.027 ± 0.002
0.67	0.193 ± 0.009	0.104 ± 0.005	0.031 ± 0.002
0.72	0.404 ± 0.021	0.190 ± 0.009	0.042 ± 0.003
0.77	0.694 ± 0.040	0.330 ± 0.018	0.045 ± 0.004

In further analysis, for each (x_F, p_T)-bin of interest, with the number of events N_{tail} in the tail region $0.16 < SX_{min} < 0.32$ cm^2 a background value N_{back} in the $SX_{min} < 0.05$ cm^2 region was defined as $N_{back} = r \times N_{tail}$.

The background as a portion of the full number of the events in the region $SX_{min} \ll 0.05\ cm^2$ versus x_F is presented in Table 6 (integrated over p_T) to make an impression of a background scale.

4.1.4. Asymmetry calculation

Asymmetry A_N has been calculated as follows:

$$A_N = \frac{1}{P_B} \times \frac{n(-) - n(+)}{n(-) + n(+)} \times \frac{n(-) + n(+)}{n(-) + n(+) - 2 \times n_{back}} , \tag{13}$$

where $n(-)$ and $n(+)$ were the numbers of the events, $N(-)$ and $N(+)$, normalized to the LOR monitors for a beam polarization vector down $(-)$ and up $(+)$, respectively. According to this definition, the asymmetry is positive when more particles are produced to the left for beam polarization up. Note that our experimental setup was on the right side of the beam axis. The n_{back} was the background defined as follows. Both the $N(-)$ and $N(+)$ SX_{min} distributions were combined to define N_{back} by scaling the ratio r on a tail of the SX_{min} summing distribution as described in the previous section. Then n_{back} was defined as N_{back} normalized to the sum of the LOR monitors for the polarization vector down and up. We can see from relation (13) that the background value n_{back} can not change a sign of A_N, however, it affects its absolute value.

The statistical accuracy σ_{A_N} included accuracies in $n(-)$, $n(+)$, and n_{back}, where σ_r was taken into account. Recall that r was defined from the experimental data (see Section 4.1.3). All statistical errors were calculated using a binomial distribution.

4.2. Time Stability of the Data

To check time stability of the data, the following was done. All the information for π^+ and π^- was broken down into several pieces, successive in time. Each part of the data corresponded to a few hours of the beam running time. Two kinematical regions were chosen, $0.55 < x_F < 0.6$ and $0.6 < x_F < 0.65$. The asymmtery in π^+ and π^- started to be non-zero in this region, and the statistics was enough to break it down to several pieces. The asymmetry was calculated for these two x_F-bins for π^+ and π^-. The results are shown in Fig.10. We have concluded that the data were stable within the errors.

4.3. Results on Cross Sections and Comparison with Earlier Experiments

The invariant cross section for particles inclusive production is given by

$$E\frac{d^3\sigma}{dp^3} = \frac{E}{2\pi p_{max} p_T} \times \frac{N_{events}}{I_{beam}} \times \frac{1}{\varepsilon} \times \frac{1}{\Delta p_T \Delta x_F} \times \frac{1}{N_n/cm^2} , \tag{14}$$

where E and p_{max} are the energy and maximum momentum of the particle, I_{beam} is the number of beam particles, which has been measured by the ionizing chamber, ε is the geometrical acceptance. The number of carbon nuclei in the target is defined as follows: $N_n = \frac{\rho l}{M} N_A = 4.4 \cdot 10^{23}\ cm^{-2}$.

This experiment didn't set the task of the cross sections measurement, therefore it was impossible to obtain the beam intensity in a real scale, the computer dead-time, the nuclear absorbtion correction etc. Despite this fact we made the calculations in some "arbitrary units" to make sure that the particles of all kinds had been reconstructed correctly and to choose the Cherenkov ADC cuts for the π^+, K^+ and protons selection.

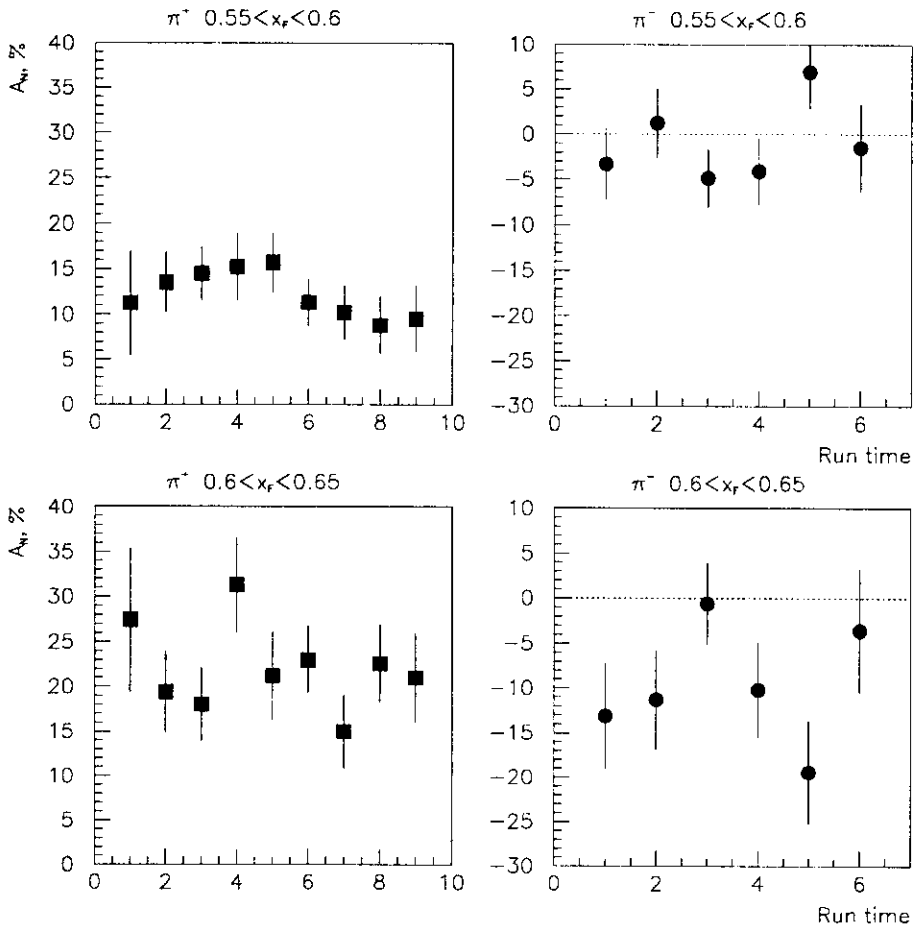

Fig. 10. Asymmetry A_N for both π^+ and π^- meson production for two x_F–bins: a) $0.55 < x_F < 0.6$ and b) $0.6 < x_F < 0.65$ as a function of beam running time. Each point corresponds to about 3 hours for π^+ and about 5 hours for π^-.

For the estimation of background interactions outside the carbon target, three special runs with the "empty" target were carried out. The "effects" ($Ef = N_{events}/I_{beam}$) at the carbon and empty target were calculated. Since their ratio $\frac{Ef_{empty}}{Ef_C}$ was about 2% in average, it didn't allow us to take into account this background.

Since a contamination of K^- and $\bar{p}$ in the π^- sample is less than 3% in our (x_F, p_T)-region, we have normalized our π^- cross section at $x_F \approx 0.53$ ($p_T \approx 0.59$), where the background from accidental coincidences in hodoscopes is small, to the one obtained on the Be target at 24 GeV [12]. Then we used this coefficient to normalize π^-, π^+ and proton cross sections in the whole x_F range. The cross sections integrated over p_T as a function of x_F are presented in Fig.11. As one can see, the form of x_F-dependence and cross sections ratios are in a good agreement with the data at 24 GeV.

We did not present the K^+-cross section because our trigger did cut part of the K^+-mesons (see a sharp left side of the K^+-spectrum in Fig.7).

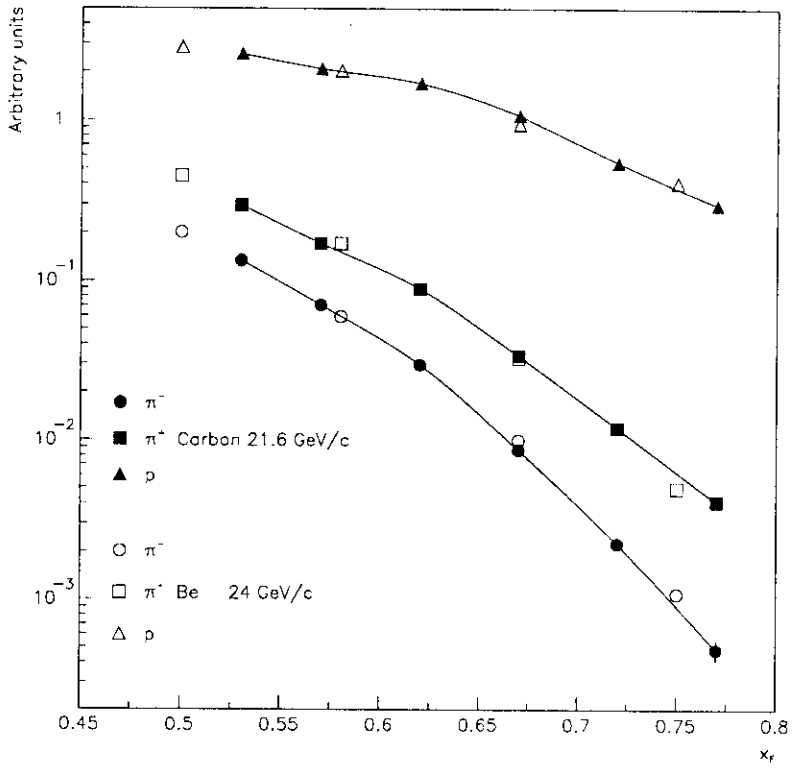

Fig. 11. Cross sections of the π^+, π^- and protons inclusive production as a function of x_F at 21.6 GeV/c in a comparison with the 24 GeV data. Curves are plotted "by eye".

4.4. Results on Asymmetries and Comparison with Earlier Experiments

The asymmetry results for all the three reactions are tabulated in Table 7 and shown in Fig.12. The data are integrated over p_T for x_F-bins. We should mention that a background can shift average numbers $< x_F >$ and $< p_T >$. Only statistical errors are presented. The main sources of point-to-point systematic errors were uncertainties in the SX_{min} region definition for asymmetry calculation and in the background estimate in the regions of interest. Study of these two factors showed that the systematic errors were a few times less than the statistical ones.

Table 7. Asymmetry A_N for π^-, π^+, and protons. Only statistical errors are presented. The details on systematic errors are in the text.

π^-			π^+			protons		
$< x_F >$	$< p_T >$ [GeV/c]	A_N [%]	$< x_F >$	$< p_T >$ [GeV/c]	A_N [%]	$< x_F >$	$< p_T >$ [GeV/c]	A_N [%]
0.48	0.51	3.2 ± 2.2	0.48	0.51	3.2 ± 1.6	0.48	0.51	-1.6 ± 3.8
0.53	0.59	2.1 ± 1.4	0.53	0.59	5.8 ± 0.9	0.53	0.58	0.5 ± 2.0
0.57	0.66	-1.6 ± 1.6	0.57	0.66	12.2 ± 1.1	0.57	0.66	2.5 ± 1.8
0.62	0.74	-9.0 ± 2.3	0.62	0.73	21.0 ± 1.6	0.62	0.73	-2.6 ± 1.8
0.67	0.81	-24.2 ± 4.2	0.67	0.81	30.4 ± 2.4	0.67	0.80	-1.1 ± 2.1
0.72	0.91	-28.8 ± 9.2	0.72	0.90	43.6 ± 4.3	0.72	0.89	2.4 ± 2.9
0.77	1.00	-47.3 ± 27.9	0.77	0.98	30.2 ± 8.6	0.77	0.96	5.9 ± 3.8

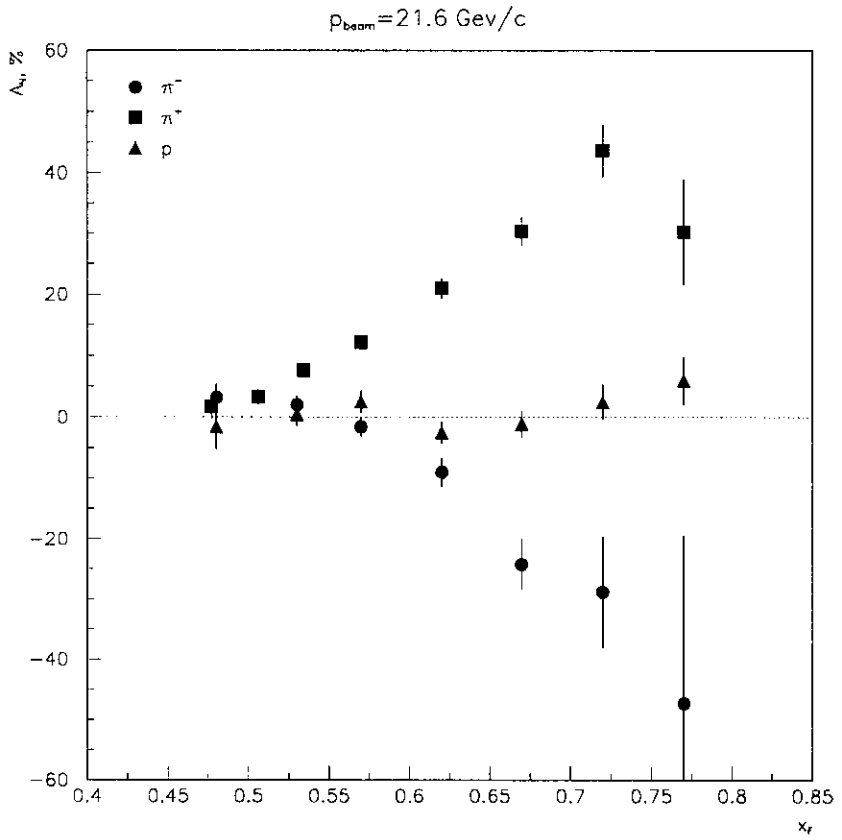

Fig. 12. Asymmetry A_N for π^-, π^+ and proton production as a function of x_F at 21.6 GeV/c.

As we know, the beam polarization magnitude P_B was defined as $0.271 \pm 0.059(stat.) \pm 0.028(syst.)$. We used the beam polarization mean value P_B only to scale A_N and σ_{A_N}. The statistical and systematic errors in P_B, taken as a quadrature, gave us a relative scale systematic uncertainty of 24% for A_N, the same for all the three reactions of interest for all x_F and p_T.

We splitted the analyzing power of π^+ in the $0.45 < x_F < 0.55$ region into three x_F-bins to look at the A_N rise in more detail. We obtained the following values (see Table 8). The statistics did not allow us to do the same for π^--mesons.

Table 8. Asymmetry A_N for π^+ at $0.45 < x_F < 0.55$.

$< x_F >$	$< p_T >$ [GeV/c]	A_N [%]
0.477	0.502	1.7 ± 2.0
0.506	0.556	3.3 ± 1.3
0.534	0.602	7.6 ± 1.1

The asymmetry A_N in π^+ and π^- inclusive production in the polarized proton beam fragmentation region at $x_F < 0.6$ was measured earlier at 13.3 and 18.5 GeV/c [13]. The x_F-dependence of A_N was presented. They observed no energy dependence. The analyzing power A_N for the π^- production is consistent with zero over the whole kinematic region up to $x_F = 0.6$. For the π^+ production, A_N rises with x_F, with an average value of about 5% in the region $x_F < 0.6$. Our results are in agreement with the results from [13].

The asymmetry A_N in π^+ and π^- production by a polarized proton beam was also measured at 11.75 GeV/c in a wide kinematic region [14]. To present their results, they used x_F and the Lorents-invariant Mandelstam variable u, the square of the four-momentum transfer from the incoming proton to the produced pion. Because they also presented momentum p_{lab} and angle θ_{lab} for each (x_F, u)-bin, we have rewritten their asymmetry in the (x_F, p_T)-bins to compare with our results. Our results in the (x_F, p_T)-bins for π^- and π^+ production are presented in Table 9 and Table 10.

Table 9. Asymmetry A_N [in %] in π^- inclusive production at 21.6 GeV/c.

x_F / p_T	0.48	0.53	0.57	0.62	0.67	0.72
0.48	-1.0 ± 3.8					
0.53	5.3 ± 3.0	1.8 ± 3.4				
0.58	1.0 ± 6.7	2.7 ± 2.0	2.6 ± 5.3			
0.63		1.7 ± 2.5	-1.6 ± 2.8			
0.68		-4.6 ± 7.2	0.2 ± 2.4	-2.8 ± 4.7		
0.73			-6.2 ± 4.4	-7.4 ± 3.7	-15.8 ± 9.2	
0.78			-25.6 ± 12.6	-16.7 ± 4.5	-23.1 ± 7.4	
0.83				-8.9 ± 7.6	-23.7 ± 8.0	-48.1 ± 16.4
0.88					-32.2 ± 9.9	-24.5 ± 15.9
0.93						-19.4 ± 18.1

Table 10. Asymmetry A_N [in %] in π^+ inclusive production at 21.6 GeV/c.

x_F / p_T	0.48	0.53	0.57	0.62	0.67	0.72
0.48	-4.6 ± 4.1					
0.53	6.2 ± 2.6	-1.5 ± 2.9				
0.58	8.0 ± 5.7	3.5 ± 1.5	8.3 ± 4.0			
0.63		12.1 ± 2.1	12.6 ± 1.9			
0.68		1.9 ± 5.9	10.8 ± 1.7	14.2 ± 3.0		
0.73			17.7 ± 3.0	22.0 ± 2.6	21.4 ± 5.6	
0.78			10.6 ± 11.8	27.6 ± 3.1	27.1 ± 4.6	
0.83				19.6 ± 5.2	37.0 ± 4.5	54.2 ± 8.7
0.88					28.8 ± 5.8	39.4 ± 7.5
0.93					47.6 ± 12.0	52.9 ± 9.2

The p_T-dependences of the A_N for π^+ and π^- mesons at some fixed x_F values are presented in Fig.13. The other way round, the x_F-dependences at some fixed p_T values are presented in Fig.14. Because the acceptance of our experimental setup was small (about 3.5% in maximum), there was a strong correlation between p_T and x_F values (see Fig.9). Strictly speaking, we do not know exactly, which particular dependences of the A_N we can see in Fig.12. Is it really an x_F-dependence? Is it a reflection of a p_T-dependence due to a narrow acceptance of the setup? Or is it a combination of the x_F and p_T-dependences? To study it, we fitted p_T and x_F-data from Fig.13 and Fig.14 by a constant and straight line. We could not find a p_T-dependence of the A_N for π^+ and π^- production at any x_F within the errors. We could not find also a x_F-dependence at $p_T \leq 0.78$ GeV/c. However, at p_T=0.83 GeV/c the data were badly fitted by a constant ($\chi^2 = 6.7$ for π^+ and 2.2 for π^-) and very well fitted by a stright line (χ^2 was

around 1 for the both π^+ and π^-). The slopes of the straight lines were 3.5σ and 2σ deviated from zero for the π^+ and π^-, correspondingly. We can conclude that we see an indication of the x_F-dependence at p_T >0.78 GeV/c. We do not see any p_T-dependence at $x_F \geq 0.57$ and any x_F-dependence at $p_T \leq$0.78 GeV/c.

We can not directly compare our π^- results with the results from [14], because the biggest p_T value at each x_F in [14] is smaller than the lowest p_T value at the same x_F in our experiment. However, the (x_F, p_T)-regions for π^+ production overlap in both experiments, and we can make a precise comparison.

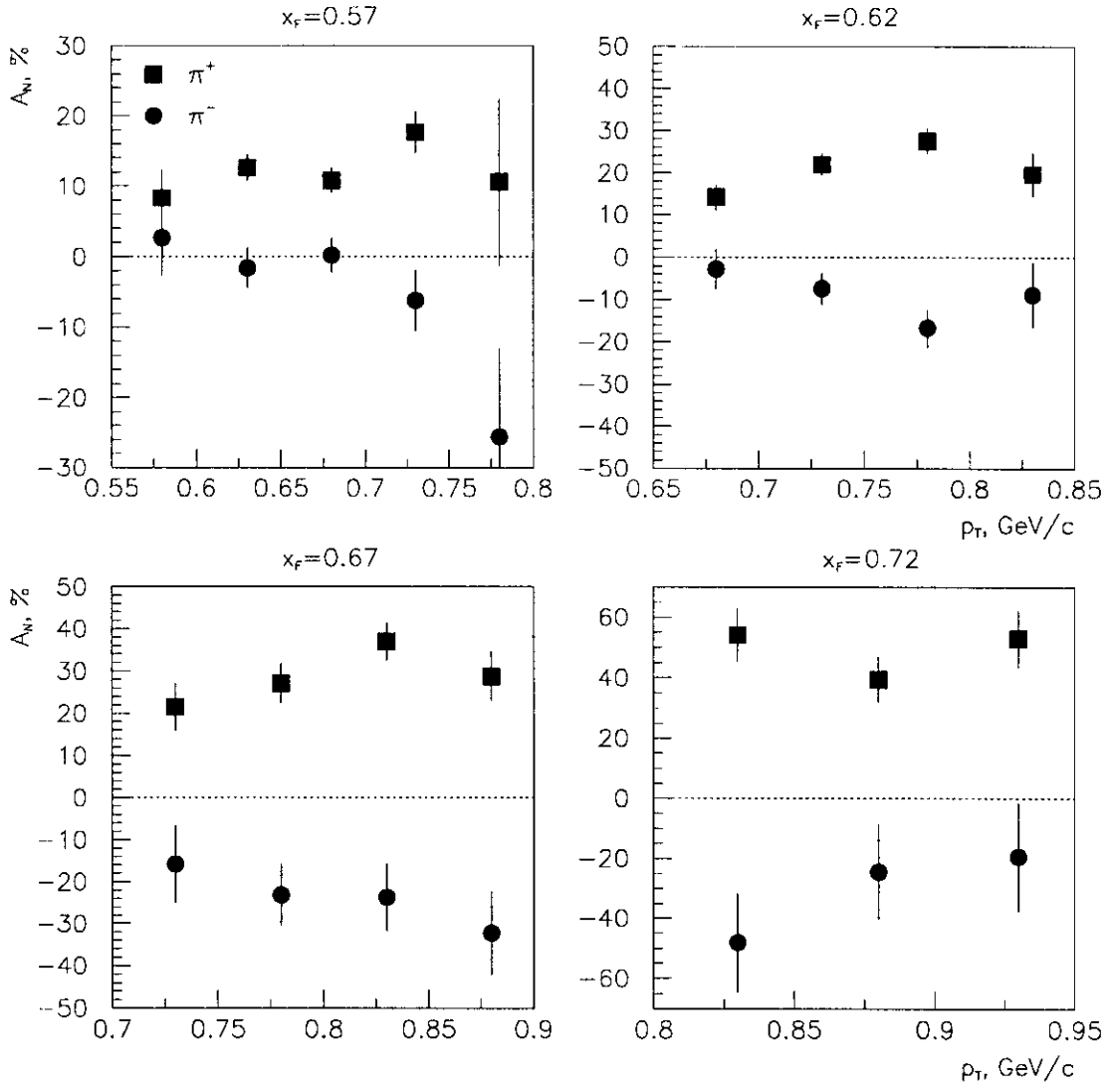

Fig. 13. The p_T−dependences of the asymmetry A_N for π^+ and π^- mesons at fixed x_F values at 21.6 GeV/c.

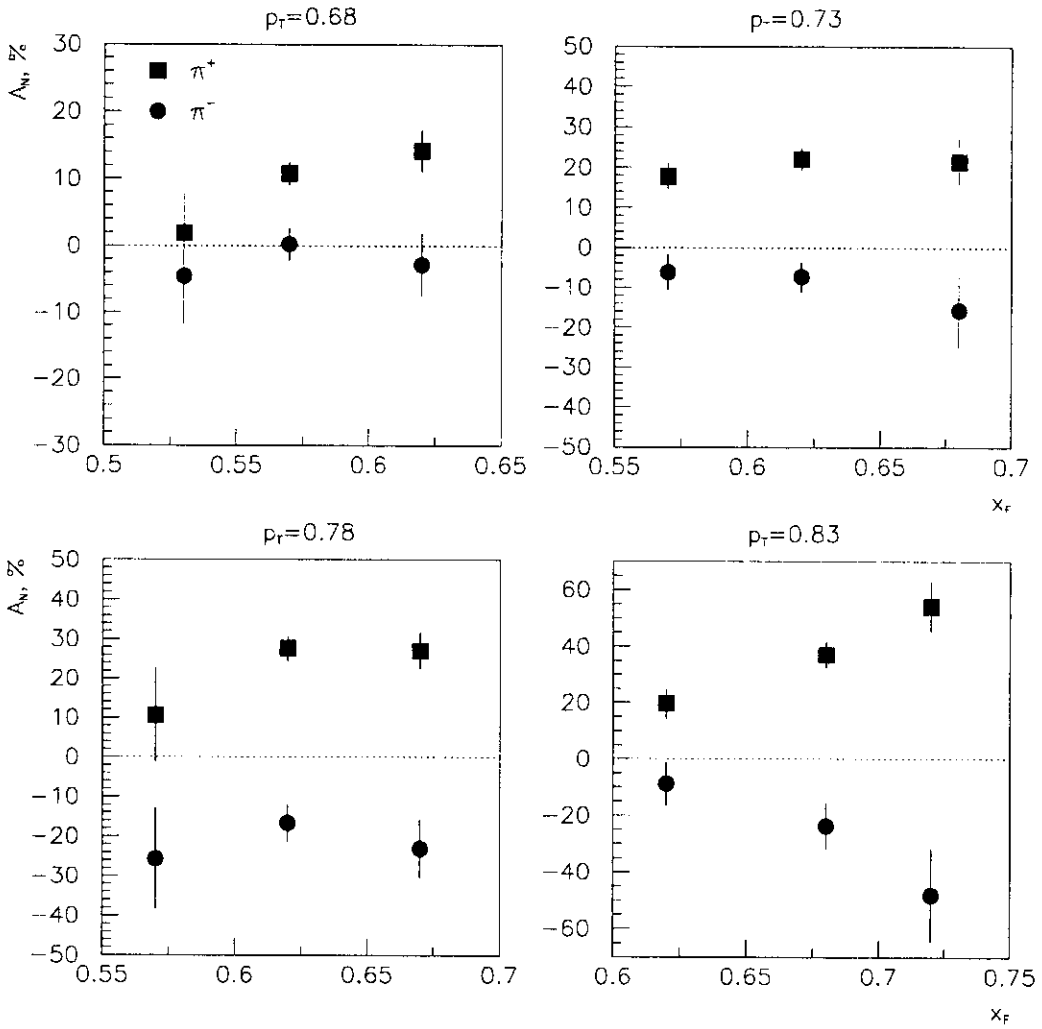

Fig. 14. The x_F−dependences of the asymmetry A_N for π^+ and π^- mesons at fixed p_T values at 21.6 GeV/c.

The results of our experiments together with the results of [14] for π^+ are presented in Fig.15 for three average $< x_F >$ values. Assuming that there is no p_T-dependence at fixed x_F, we can calculate average A_N values over presented in Fig.15 p_T regions at three x_F values for both the sets of the data, and come up with an x_F-dependence of the asymmetry. The results are plotted in Fig.16. We can see that the analyzing power A_N for π^+ mesons at 21.6 GeV/c is bigger than the A_N at 11.75 GeV/c.

After all, we should compare our data with the results of E704 [1]. We fitted both of the data sets by straight lines. Results are shown in Fig.17. One can see two peculiarities: both the x_F values where A_N approach zero and the slopes of fitting lines, dA_N/dx_F, are larger at 21.6 GeV/c in comparison with the 200 GeV/c data. However, we should point out differencies in target species (carbon vs. hydrogen) and the p_T acceptances of the two experiments. Asymmetries for π^+ and π^- at these two beam momenta are approximately equal in the large x_F region ($x_F > 0.6$), which will be the kinematic range for the polarimetry.

The asymmetry A_N for protons in the (x_F, p_T)-bins is given in Table 11. We could not see non-zero asymmetry in any (x_F, p_T)-region.

Table 11. Asymmetry A_N [in %] in proton inclusive production at 21.6 GeV/c.

x_F / p_T	0.48	0.53	0.57	0.62	0.67	0.72
0.48	2.9 ± 8.1					
0.53	-1.2 ± 4.6	-7.0 ± 5.0				
0.58	-12.0 ± 11.8	2.1 ± 2.6	3.8 ± 6.0			
0.63		0.1 ± 4.0	2.8 ± 3.0	-5.0 ± 10.0		
0.68		1.9 ± 11.9	-0.2 ± 2.8	-2.2 ± 3.4		
0.73			6.3 ± 4.9	-1.3 ± 3.2	-4.8 ± 4.6	
0.78				-6.1 ± 3.8	3.3 ± 4.1	6.5 ± 9.6
0.83				1.6 ± 6.0	-0.8 ± 4.2	6.1 ± 6.1
0.88					-7.1 ± 5.4	4.6 ± 5.4
0.93					9.2 ± 9.3	-0.4 ± 6.2

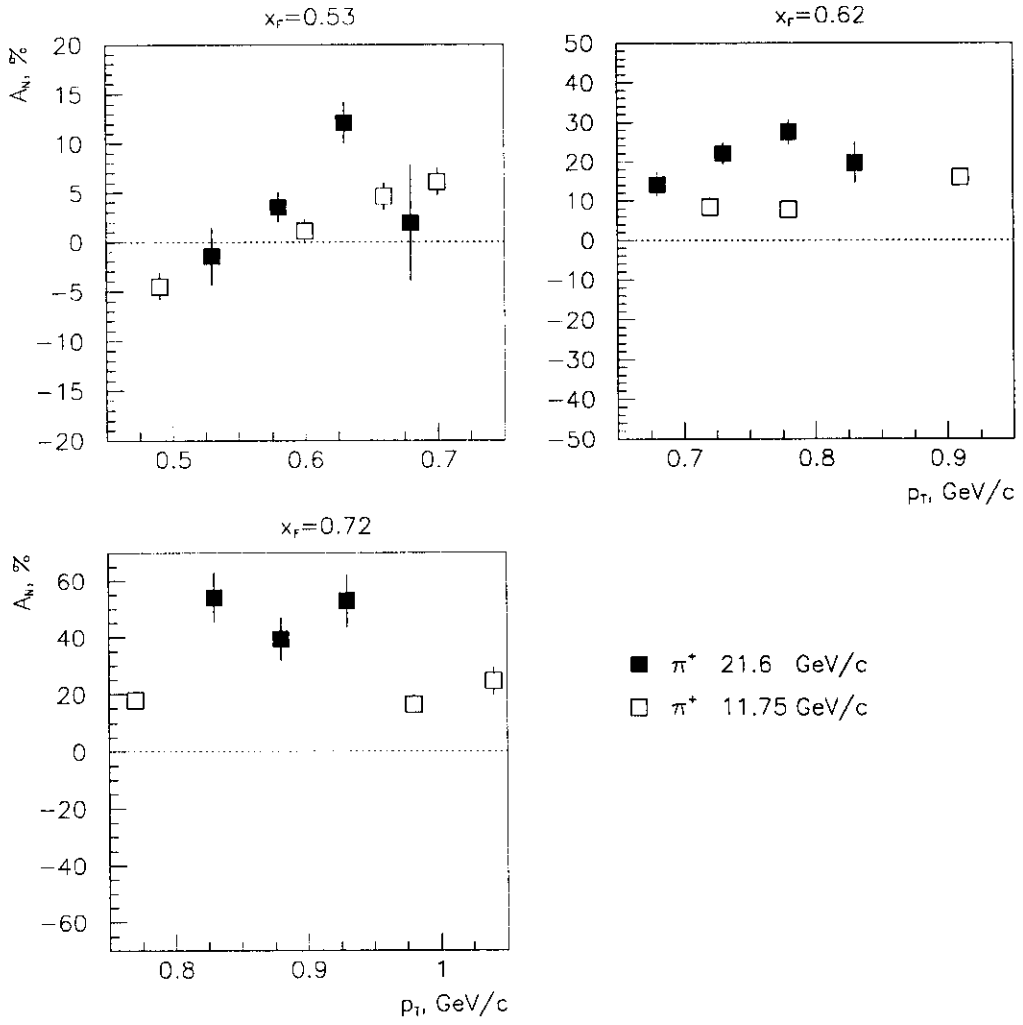

Fig. 15. Comparison of the 21.6 GeV/c π^+ data and the 11.75 GeV/c π^+ data [14] at some fixed x_F values.

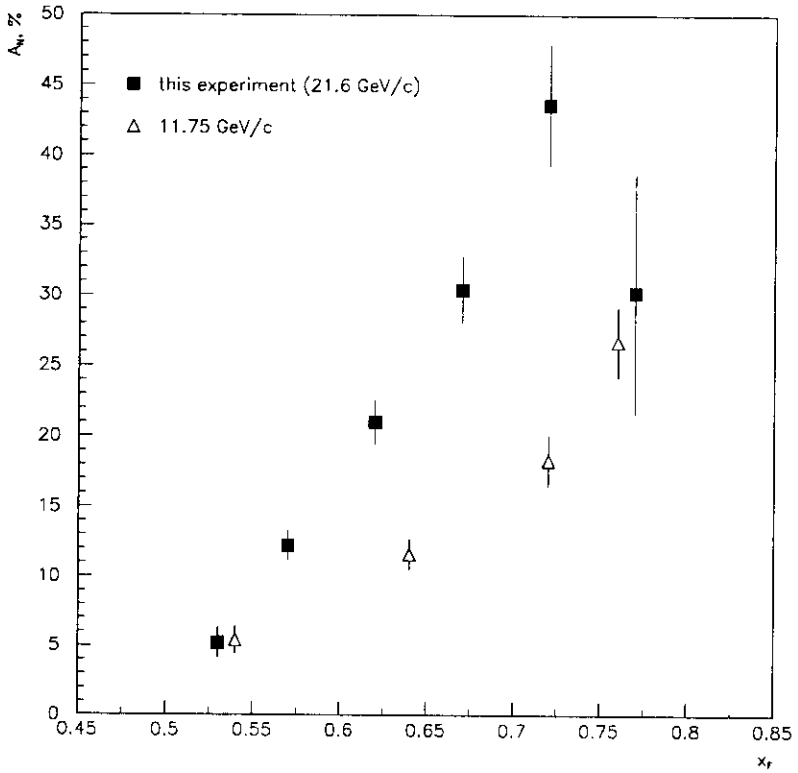

Fig. 16. The x_F–dependences of the asymmetry A_N at 21.6 GeV/c and 11.75 GeV/c [14] in the overlapped p_T regions. See details in the text.

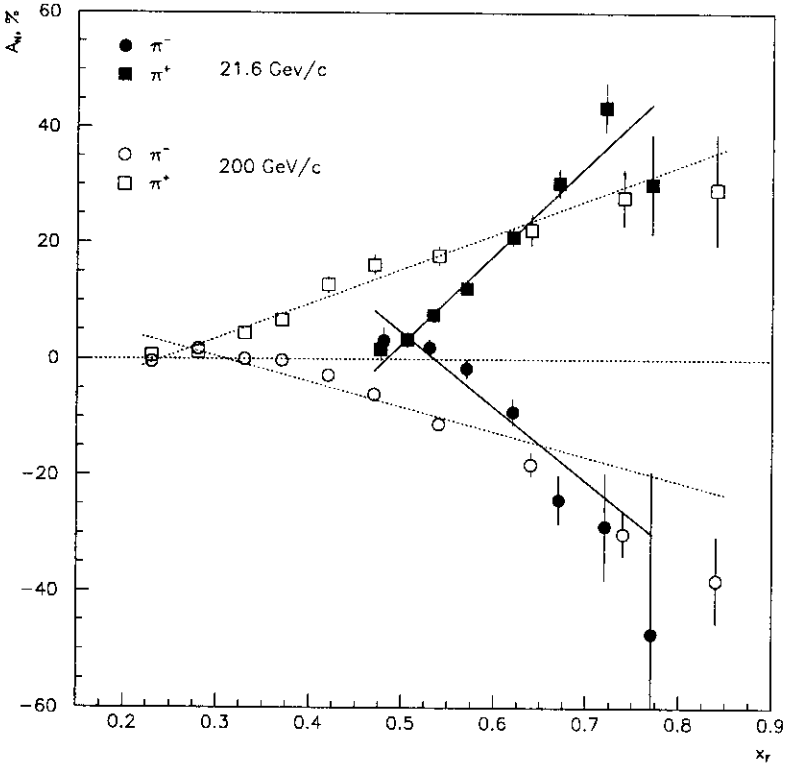

Fig. 17. Comparison of the 21.6 GeV/c and 200 GeV/c [1] data.

4.5. False Asymmetries

To study a false asymmetry all the criteria from Table 4 were applied, except the SX_{min} one. We used $SX_{min} > 0.05$ cm^2 region to calculate the false asymmetry by using expression (13), but obviously no background subtraction in the denominator was made. The results are shown in Table 12.

Table 12. False asymmetry [in %] for π^-, π^+ and protons. $SX_{min} > 0.05$ cm^2.

$< x_F >$	π^-	π^+	protons
0.48	8.8 ± 6.9	5.9 ± 6.4	-16.0 ± 13.3
0.53	0.9 ± 4.4	10.9 ± 3.6	-9.9 ± 7.3
0.57	-1.1 ± 4.9	7.1 ± 3.6	-5.2 ± 6.6
0.62	-6.7 ± 5.8	8.3 ± 4.7	-5.4 ± 7.2
0.67	-2.5 ± 7.1	11.2 ± 5.6	-10.8 ± 7.4
0.72	8.3 ± 8.5	6.1 ± 7.5	21.5 ± 9.8
0.77	10.7 ± 9.9	0.1 ± 9.9	3.9 ± 12.8
average $x_F > 0.45$	0.8 ± 2.3	8.4 ± 1.9	-4.4 ± 3.1
average $x_F > 0.55$	-0.6 ± 3.0	7.6 ± 2.3	-2.3 ± 3.6

We concluded that we did not see a false asymmetry in π^- and protons, but there is a false asymmetry in π^+. By studing the region $0.05 < SX_{min} < 0.1$ cm^2, we found that the asymmetry for π^+ was only about twice smaller than A_N in the region $SX_{min} < 0.05$ cm^2. It can be explained by the fact that one half of the events in this region is still π^+'s, and another half is a background. The region $x_F > 0.55$ is specially pointed out in Table 12, because there is zero or small asymmetry A_N in all the three reactions at $x_F < 0.55$. We reinforced our SX_{min} cut. The results are presented in Table 13.

Table 13. False asymmetry [in %] for π^+. $SX_{min} > 0.1$ cm^2.

$< x_F >$	π^+
0.48	1.7 ± 10.8
0.53	19.7 ± 6.4
0.57	8.8 ± 5.9
0.62	5.5 ± 7.2
0.67	3.6 ± 8.1
0.72	-8.0 ± 9.8
0.77	0.0 ± 12.6
average $x_F > 0.45$	7.3 ± 3.0
average $x_F > 0.55$	4.1 ± 3.5

As we can see from Table 13, in the region $SX_{min} > 0.1$ cm^2 and $x_F > 0.55$ the false asymmetry decreased. We can conclude that it is zero within the errors. To make sure that the false asymmetry of the background is zero, we have further strengthened the SX_{min} cut. The results of the false asymmetry for the $SX_{min} > 0.16$ cm^2 region are summarized in Table 14.

Table 14. False asymmetry [in %] for π^+. $SX_{min} > 0.16$ cm^2.

$< x_F >$	π^+
0.48	-21.9 ± 16.5
0.53	9.6 ± 9.1
0.57	2.3 ± 8.1
0.62	6.8 ± 9.7
0.67	3.4 ± 10.6
0.72	-13.0 ± 12.6
0.77	11.1 ± 15.7
average $x_F > 0.45$	2.2 ± 4.1
average $x_F > 0.55$	2.2 ± 4.7

The false asymmetry for π^+ production is zero within the errors in the whole x_F-region in the backgound tail region at $SX_{min} > 0.16$ cm^2. Earlier we saw that the false asymmtery for π^- and protons is zero within the errors at all x_F already in the $SX_{min} > 0.05$ cm^2 region. All this proves that in equation (13) we can consider that the background n_{back} does not have an asymmetry.

4.6. Discussion of Theoretical Models for Asymmetries

From recent experiments it is known that mesons produced in spin polarized proton-proton(nuclear) collisions at medium and high energies exhibit significantly large asymmetry at large x_F in a small p_T region. Our results at 21.6 GeV/c confirm this statement. Large polarizations were also observed in hyperon production. There is a common beliefe that the asymmetries in meson and polarization in hyperon production are related. In these observations, the long-range part of the strong interaction may play an important role. Study of the mechanism producing such a large asymmetry in meson production is expected to provide important information on spin-dependent quark dynamics, momentum distributions of constituents, hadronization, and quark confinment. Up to now, however, there is no rigorous model which enables us to interpret systematically the properties of all these polarization effects. Various theoretical mechanisms were proposed recently to explain significant asymmetries observed in pion production: higher twist effects [15], correlation of $k_\perp$ and spin in structure [16] and fragmentation [17] functions, rotation of valence quarks inside a hadron [18,20], a role of the orbital angular momentum [20], quark recombination model with a relativistic description for the parton-parton interaction [4]. Also there are a lot of various phenomelogical models proposed on this point which are based on different assumptions for the quark dynamics [21,22,23,24]. At small p_T, the quark recombination picture [25,26] is the most likely model to produce hyperons in high energy proton-proton collisions. This model is known to reproduce the experimental tendencies of spin observables in the inclusive hadron reactions.

A model by Meng and Liang [19] explains the asymmetry in mesons production by a correlation between the spin of the proton and the orbital motion of the valence quarks. The u-valence quarks are more likely to be polaried in the same direction as the proton spin, whereas the d-valence quark is more likely to be polarized in the opposite direction to the proton spin. When the surfaces of a polarized beam proton and unpolarized target proton come into contact, a π^+ will form a valence u quark and a sea $\bar{d}$ quark and go left (with higher probability) when

the polarization is up. A π^- will form from a valence d quark and a sea $\bar{u}$ quark and go right (with higher probability) when the polarization is up. Their model matches the data at least qualitatively and may provide an interesting way to picture the physics causing the asymmetry.

In a model by Troshin and Tuyrin [20] the main role in the generation of the asymmetries in inclusive π-production belongs to the orbital angular momentum of the quark-antiquark cloud in the internal structure of constituent quarks. The x_F-dependence of asymmetries in $\pi^{\pm}$-production at large x_F reflects the corresponding dependence of constituent quark polarization in the polarized proton. The model described well the large x_F asymmetries at 200 GeV.

The relativistic formulation of the quark recombination model for polarizations of hyperons and mesons [4] reproduce successfully both the E704 inclusive pion data and numerous hyperon polarization results.

Another model by Anselmino et al. [27] explains the pion asymmetry using the perturbative QCD. They consider the role of the parton intrinsic $k_\perp$ in the initial polarized proton. They conclude that although leading twist effects vanish in single spin asymmetries, higher twist effects may be important. They are able to reproduce the main features of the 200 GeV pion data with their model. Other work also supports the idea that twist-3 contributions can lead to non-zero asymmetries [28]

Recent paper by Qiu and Sterman [29] predicts an A_N dependence at large x_F, based on a "valence quark–soft gluon" approximation. The twist-3 parton correlation functions that couple quark and gluon fields become important in the large x_F region; lower order twist-2 effects do not contribute to A_N. Their theory seems to predict only a slow change with energy for a given p_T, and explain the gross features of both the 22 and 200-GeV/c data.

5. CONCLUSION

A large analyzing power was observed in π^+ and π^- inclusive production at 22 GeV/c with the use of a polarized beam for $x_F > 0.5$ and $0.6 < p_T < 1.2$ GeV/c.

The signs of the inclusive pion production asymmetries are found to be the same at 22 GeV/c as at 200 GeV/c. The data at both 22 and 200 GeV/c exhibit an approximate mirror symmetry as a function of x_F. Data at lower momenta for π^+-mesons are consistent in sign and show a similar rise with x_F. We can not compare directly our π^--asymmetry with the one at low energies, because of different kinematic (x_F, p_T)-regions covered by the experiments.

The values of x_F where the $\pi^{\pm}$-analyzing powers approach zero moves with beam momentum. These zero points are independent of systematic errors on the magnitude of A_N. The values of x_F where A_N extrapolates to zero and the slopes are both larger at 22 GeV/c for a carbon target than at 200 GeV/c for a hydrogen target. There is a difference in both the target (carbon versus hydrogen) and momentum (22 versus 200 GeV/c) between the E925 and E704 results. There is also a difference in the acceptances, the E925 acceptance is narrower than the one in the E704.

Inclusive proton production exhibits no measurable asymmetry at 22 GeV/c. Some lower-energy proton data show a small asymmetry (up to 5%) for a target of hydrogen and deuterium.

The data in this paper will complement the extensive hyperon polarization results, and should provide a better understanding of the mechanisms leading to a large spin effect at high energy. These data present the first strong indication for large and nearly energy independent analyzing powers at high x_F ($x_F > 0.6$) in inclusive $\pi^{\pm}$-production in the energy range between 22 and 200 GeV. This may allow these reactions to be used for high energy proton beam polarimeters, such as for RHIC and HERA.

ACKNOWLEDGMENTS

We are grateful to the AGS staff for their assistance with setting up the experiment and operating the accelerator. This project was supported in part by the U.S. Department of Energy, Division of High Energy Physics, Contracts W-31-109-ENG-38 and DE-FG02-92ER40747, and the Russian Ministry of Science and Technology. A portion of this research was performed in the framework of the RIKEN-BNL collaboration for the RHIC-Spin project.

References

[1] D.L. Adams *et al.*, Phys.Lett. **B264**, 462 (1991)

[2] K. Heller, Proceedings of the 12th International Symposium on High-Energy Spin Physics, Amsterdam, (eds. C.W. de Jager *et al.*, World Scientific), p.23 (1996)

[3] Z. Liang and C. Boros, Phys.Rev.Lett. **79**, 3608 (1997)

[4] Y. Yamamoto, K. Kubo, and H. Toki, Prog.Theor.Phys. **98**, 95 (1997)

[5] H. Spinka *et al.*, Nucl. Instr. and Meth. **211** , 239 (1983).

[6] D.G. Crabb *et al.*, Nucl. Phys. **B121** , 231 (1977).

[7] M. Borghini *et al.*, Phys.Lett. **B36**, 501 (1971).

[8] A. Gaidot *et al.*, Phys.Lett. **B61**, 103 (1976)

[9] C. Ohmori *et al.*, Nucl. Instr. and Meth. **A278** , 705 (1989).

[10] N. Akchurin *et al.*, Phys. Lett. **B229**, 299 (1989).

[11] A.I. Pavlinov, preprint IHEP 98-37, Protvino (1998)

[12] I. Eichten *et al.*, Nucl.Phys. **B44**, 333 (1972)

[13] B.E. Bonner *et al.*, Rhys.Rev. **D41**, 13 (1990)

[14] W.H. Dragoset *et al.*, Phys.Rev. **D18**, 3939 (1978)

[15] A.V. Efremov and O.V. Teryaev, Sov.J.Nucl.Phys. **36**, 140 (1982); J. Qiu and G. Sterman, Nucl.Phys. **B378**, 52 (1992); S.J. Brodsky, P. Hoyer, A.H. Mueller, and W.-K. Tang, Nucl.Phys. **B369**, 519 (1992).

[16] D. Sivers, Phys.Rev. **D41**, 83 (1990), **D43**, 261 (1991); M. Anselmino, M.E. Bologlione, and Murgia, High Energy Spin Physics, edited by K. Heller and S. Smith, AIP Conf.Proc.343 (AIP, New York, 1994), p.446.

[17] J.C. Collins, Nucl.Phys. **B396**, 161 (1993); J.C. Collins, S.F. Heppelman, and G.A. Ladinsky, Nucl.Phys. **B420**, 565 (1994).

[18] C. Boros, Z. Liang, and Meng Ta-chung, Phys.Rev.Lett. **70**, 1751 (1993).

[19] Z. Liang and T. Meng, Z.Phys. **A344**, 171 (1992).

[20] S.M. Troshin and N.E. Tyurin, Phys.Rev. **D54**, 838 (1996).

[21] T.A. DeGrand and H.I. Miettinen, Phys.Rev. **D23**, 1227 (1981),**D24**, 2419 (1981), **D31**, 661 (1985).

[22] B. Andersson, G. Gustafson, and G. Ingelman, Phys.Lett. **B85**, 417 (1979).

[23] J. Soffer and N.A. Torngvist, Phys.Rev.Lett. **68**, 907 (1992).

[24] R. Lednicky, Sov.J.Nucl.Phys. **43**, 817 (1986); P. Cea *et al.*, Phys.Lett. **B193**, 361 (1987); M.G. Ryskin, Sov.J.Nucl.Phys. **48**, 708 (1988); T. Fujita and N. Suzuki, Nucl.Phys. **A503**, 899 (1989); W.G.D. Dharmarratna and G.R. Goldstein, Phys.Rev. **D41**, 1731 (1990); M. Svec, Phys.Rev. **D42**, 2237 (1990).

[25] K.P. Das and R.C. Hwa, Phys.Lett. **B68**, 459 (1977).

[26] R.C. Hwa, Phys.Rev. **D22**, 1593 (1980).

[27] M. Anselmino *et al.*, Phys.Lett. **B362**, 164 (1995).

[28] P. Ratcliffe, submitted to Euro.Phys.J. C, June 1998.

[29] J. Qiu and G. Sterman, preprint HEP-PH/9806356 (1998).

Received March 18, 1999

Contents

К.Аллговер и др.
Измерение односпиновой асимметрии в инклюзивном образовании π^+, π^- и протонов на углеродной мишени с использованием поляризованного протонного пучка с импульсом 21.6 GeV/c. (Эксперимент E925 БНЛ).

Оригинал-макет подготовлен с помощью системы LaTeX.
Редактор Е.Н.Горина. Технический редактор Н.В.Орлова.

Подписано к печати 22.03.99. Формат 60 × 84/8. Офсетная печать.
Печ.л. 3.87. Уч.-изд.л. 3.1. Тираж 160. Заказ 103. Индекс 3649.
ЛР №020498 17.04.97.

ГНЦ РФ Институт физики высоких энергий
142284, Протвино Московской обл.

Индекс 3649

П Р Е П Р И Н Т 99-14, И Ф В Э, 1999